UNITED STATES NAVAL ACADEMY
Annapolis, Maryland 21402-5041

DIVISION OF ENGINEERING AND WEAPONS

Report EW-03-01

ENGINEERING SUPPORT FOR THE DEVELOPMENT OF A SUBMERSIBLE FISH CAGE FOR OPEN OCEAN AQUACULTURE

David W. Fredriksson, Ph.D.[1]
Judson DeCew,[2]
Chad Turmelle,[2]
James D. Irish, Ph.D.[3]

[1]Assistant Professor
Department of Naval Architecture and Ocean Engineering
United State Naval Academy
Annapolis MD, 21108

[2]Research Engineer
Department of Mechanical Engineering
University of New Hampshire
Durham NH 03824 USA

[3]Research Professor
Center for Ocean Engineering
University of New Hampshire
Durham NH 03824 USA

Report Documentation Page

Form Approved
OMB No. 0704-0188

1. REPORT DATE	2. REPORT TYPE	3. DATES COVERED
2007		**00-00-2007 to 00-00-2007**

4. TITLE AND SUBTITLE	5a. CONTRACT NUMBER
Engineering Support for the Development of a Submersible Fish Cage for Open Ocean Aquaculture	5b. GRANT NUMBER
	5c. PROGRAM ELEMENT NUMBER
6. AUTHOR(S)	5d. PROJECT NUMBER
	5e. TASK NUMBER
	5f. WORK UNIT NUMBER
7. PERFORMING ORGANIZATION NAME(S) AND ADDRESS(ES) **United States Naval Academy (USNA),Department of Naval Architecture and Ocean Engineering,Annapolis,MD,21402**	8. PERFORMING ORGANIZATION REPORT NUMBER
9. SPONSORING/MONITORING AGENCY NAME(S) AND ADDRESS(ES)	10. SPONSOR/MONITOR'S ACRONYM(S)
	11. SPONSOR/MONITOR'S REPORT NUMBER(S)

12. DISTRIBUTION/AVAILABILITY STATEMENT
Approved for public release; distribution unlimited

13. SUPPLEMENTARY NOTES

14. ABSTRACT

15. SUBJECT TERMS

16. SECURITY CLASSIFICATION OF:			17. LIMITATION OF ABSTRACT	18. NUMBER OF PAGES	19a. NAME OF RESPONSIBLE PERSON
a. REPORT	b. ABSTRACT	c. THIS PAGE			
unclassified	**unclassified**	**unclassified**	**Same as Report (SAR)**	**43**	

Executive Summary

The objective of this project was to utilize the University of New Hampshire, Open Ocean Aquaculture (OOA) facility to examine the performance of a new fish cage system. The fish cage was constructed with High Density Polyethylene pipe as lower and upper structural rim components. The two rim assemblies are connected using knotless net and triangular stays. Below the cage is an airlift assembly and ballast chain. The system was deployed at the exposed OOA site in the Gulf of Maine with a 4-bay, submerged grid mooring system. Two other fish cages, along with a feed buoy were also deployed within the mooring system.

The goal of the field portion of the study was to examine how the new cage would survive open ocean conditions. To help quantify survival, inline load cells were installed with the attachment lines to measure loads on the surface rim. Wave and currents were also measured at the site to quantify the forcing. The field data sets were needed to investigate finite element modeling approaches so that extreme conditions could be simulated. The finite element model used in this study calculates mooring system can cage attachment loads. Environmental parameters input to the model included waves and currents that were measured at the site. Calculation results were compared with loads measured in-situ. Simulations were then performed using a more extreme case in an effort to understand what type of loads the cage structure could withstand.

Table of Contents

1. Introduction

The work described in this paper represents the culmination of a 10-year vision to develop a fully instrumented open ocean facility for the testing of novel marine aquaculture technologies at the University of New Hampshire (UNH). In this study, a Small Business Innovation Research (SBIR) grant was awarded from the National Oceanic and Atmospheric Administration (NOAA) to a company called JPS Industries to develop a fish cage for open ocean aquaculture. One of the objectives was to test the fish cage at the open ocean site while measuring forcing and response parameters. Another objective was to develop a model representation of the fish cage using the program Aqua-FE validated with the field measurements. The Aqua-FE program is a finite element modeling tool for evaluating marine aquaculture systems (Tsukrov et al., 2003; 2005) The model was used to calculate loads on the system for the most extreme environmental conditions during the deployment period.

The fish system was designed using sections of High Density Polyethylene (HDPE) pipe with components capable of being ballasted for submerged operations. As part of a companion study, the attachment loads measured and calculated were then used as input to a structural numerical model of the fish cage using a commercially available software package called MSC.MENTAT. Using the localized failure technique described in Fredriksson et al. (2007a), cage rim stresses were determined for proper component specification to prevent system failure and escapement. These loads can also be used with visual observations of wear on the components are incorporated into future designs.

The approach in this study was to perform field measurements for comparison with results from the Aqua-FE model of the system and determine the maximum cage attachment load that current during a specific extreme condition. Field measurements were performed at the open ocean aquaculture (OOA) testing site located approximately 10 km from the New Hampshire (NH) coastline, about 2 km south of the Isles of Shoals (Figure 1). At the site, a submerged four bay grid mooring system was installed in 2003 for the purposes of testing novel OOA systems (Fredriksson et al. 2004). In this study, the new cage system was deployed in one of the grid bays and attached to the cage mooring with in-line load cells to measure attachment tensions. To quantify the forcing mechanisms, oceanic currents and waves were measured from a nearby monitoring buoy. Additional weather information was obtained from National Data Buoy Center

(NDBC) installations at the Isles of Shoals (Station IOSN3) and Buoy BO102 (Station 44030). Data sets from the field measurements where then analyzed for suitable load cases that could be used as input in the Aqua-FE model.

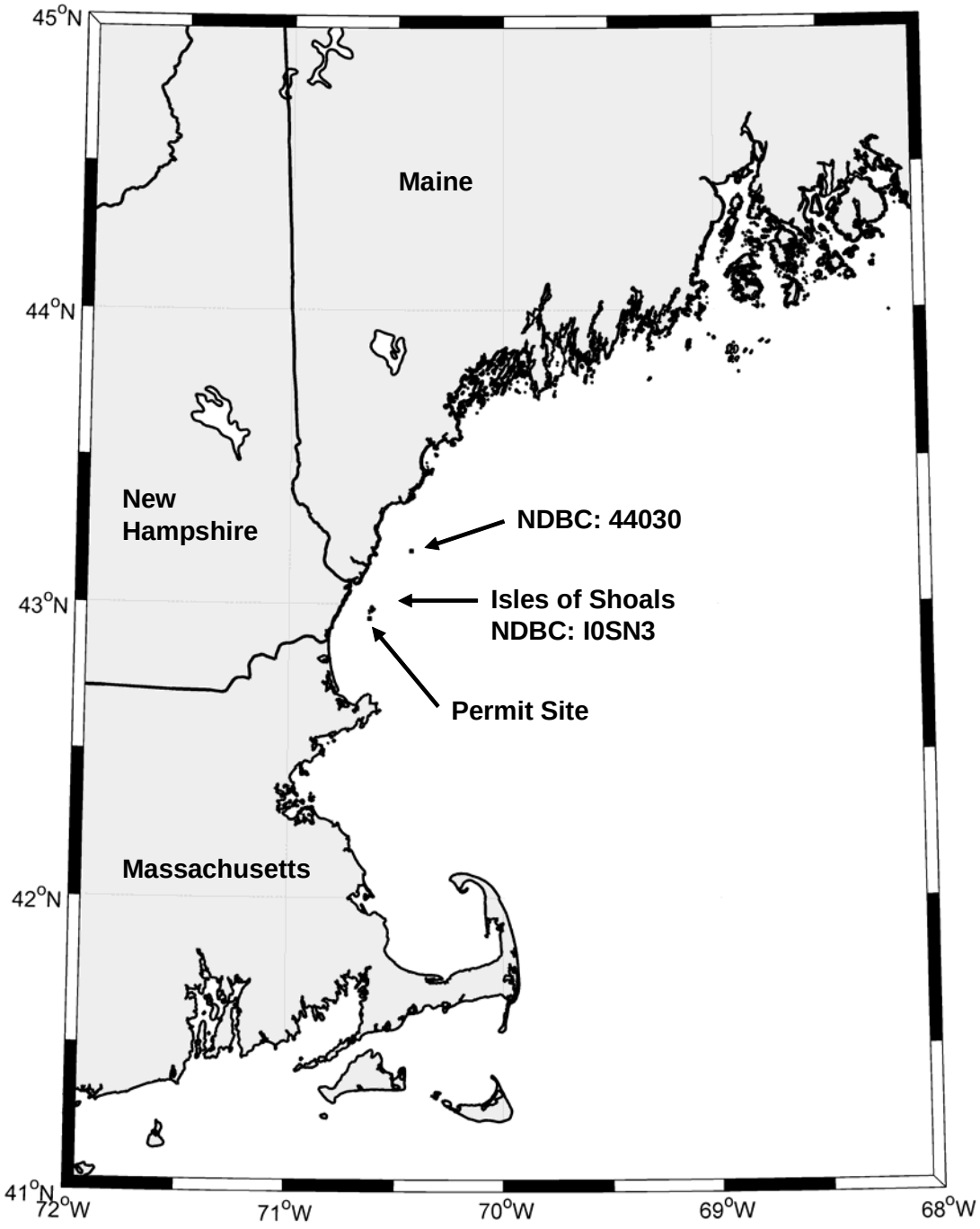

Figure 1: Location of the aquaculture site operated by the (UNH). Also shown on the Figure are the Isles of Shoals and the National Data Buoy Center site 44030.

2. Marine Aquaculture System

The fish cage being developed as part of the SBIR project was constructed using upper and lower rim assemblies held together with angled stays. Both rim assemblies were made with straight sections of HDPE pipe with custom designed connectors. Construction details are provided in Santamaria et al. (2007), (2006a) and (2006b) and summarized in Appendix A. These two structural components maintain the shape of the net chamber used to contain the fish. The upper rim contains both fixed and variable buoyancy, while the lower rim is weighted. Suspended below the lower rim are a set of bridles that connect to an airlift. Below the airlift is ballast line and chain. A general schematic of the SBIR cage design is shown on Figure 2.

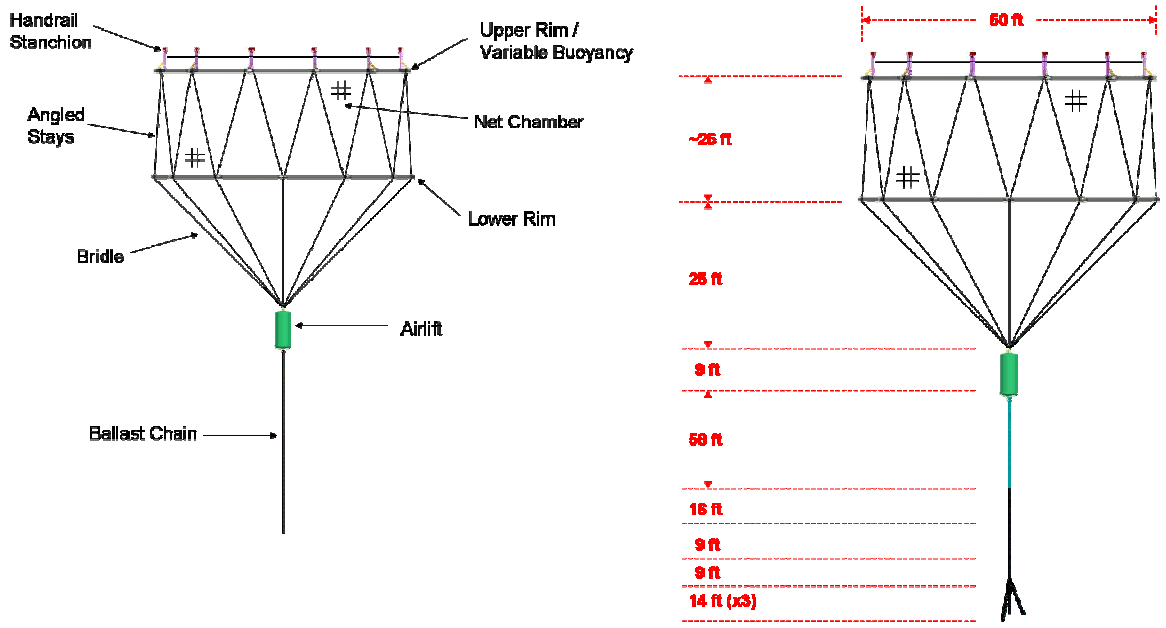

Figure 2: SBIR cage design. The upper rim sections support the net chamber and lower rim (via angled stays). An airlift and ballast chain hangs from a bridle off the lower rim. The cage has two ballasting systems (for test purposes) located in the upper rim section and airlift.

Another component of the system includes a feed hose buoy used to deliver pellets to fish in the cage while the system is submerged. Since the feed hose buoy was not critical in the development of the fish cage system, a prototype was not built (to save project funds for fish cage construction), but a design was completed within the first year of the project. A dimensioned schematic with an exploded view is shown on Figure 3. The design consists of a cylindrical foam section surrounding a length of pipe (4 inch, schedule 40, aluminum). The bottom portion (below the surface) of the pipe is flanged so that a flexible hose can be attached

with other end connect to the cage. The top portion of the pipe (above the surface) has a quick release fitting so that a hose can be attached and feed slurry pumped down to the cage. The buoy contains a superstructure (also made of aluminum) for mounting radar reflectors, lights and solar panels. The superstructure contains enough space for a battery and control system if remote monitoring of the cage is necessary. The monitoring system would be connected to the cage through conductors incorporated in a flexible hose, as similar to those described in Paul (2004). Another option would be to send signal down a coil cord assembly wrapped around the hose (Irish et al, 2005). A complete component listing of the feed hose buoy is provided in Appendix B. The feed hose buoy was not deployed as part of this modeling study.

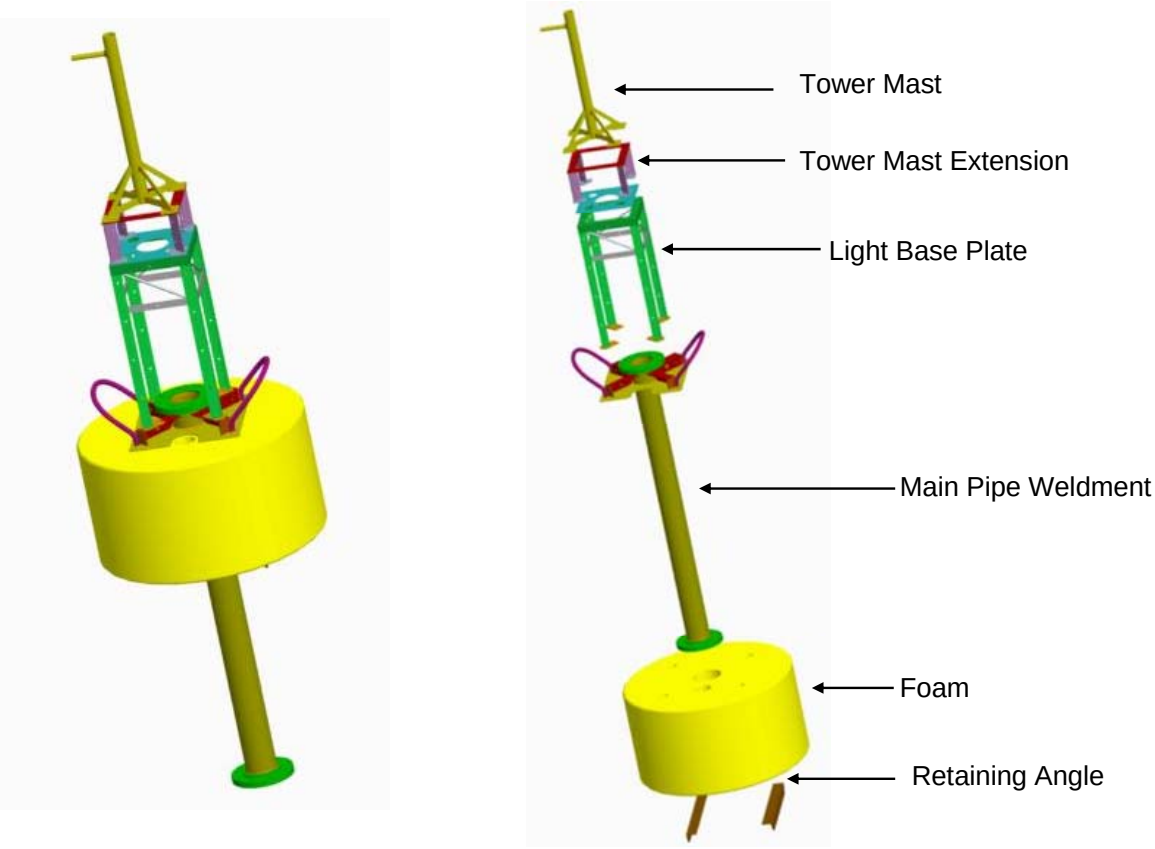

Figure 3: Components of the feed hose buoy.

As previous mentioned, the SBIR cage was deployed at the OOA site. The site, however, is utilized as a testing area for many kinds of exposed aquaculture research. For instance, also deployed within the mooring system were two SeaStation cages, one having a volume a 600 m^3 (SS600) and the other a volume 3000 m^3 (SS3000), though the smaller cage was deployed

without a net. Mooring and cage construction details are provided in Fredriksson et al. (2004). A feeding buoy was also deployed at the site as with component details described in Fullerton et al. (2004).

3. Field Measurement Program

3.1. Overview

From June to November 2006, the prototype SBIR cage was deployed at the OOA site in the four-bay grid mooring. The SBIR cage was connected to the mooring system using four sets of attachment line assemblies (Figure 4). The attachment lines on the northeast and southeast side of the cage incorporated two in-line load cells, called NE and SE, respectively. The mooring system, SeaStation Cages, operational feed buoy and the SBIR cage that were deployed at the site, were all components represented in the Aqua-FE model portion of the study.

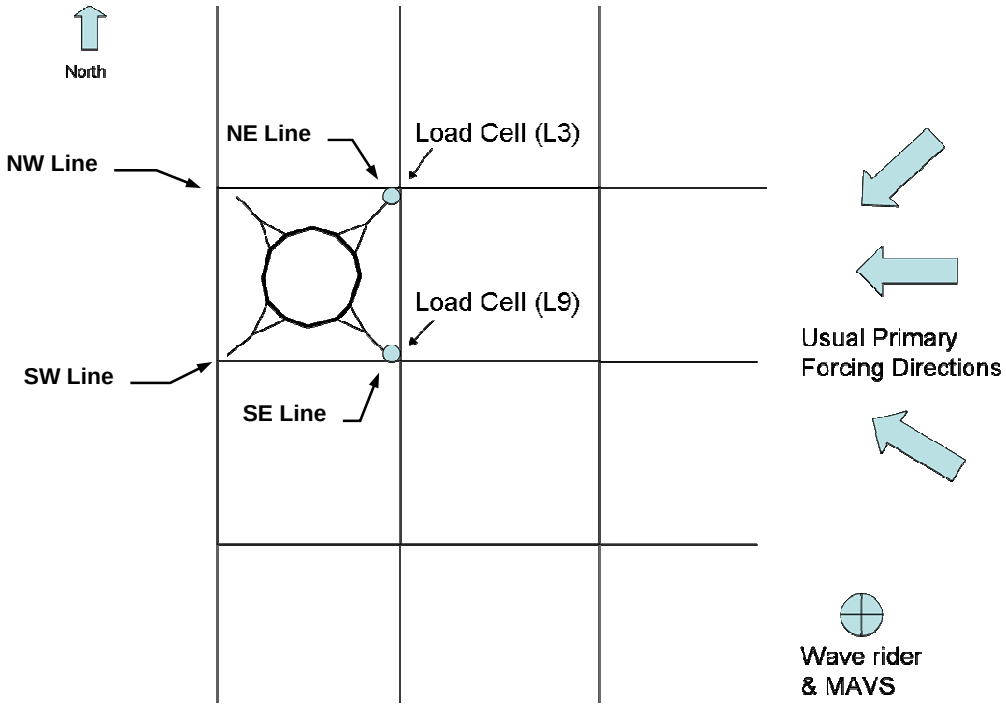

Figure 4: The locations of the instrumentation at the OOA site. Note that the feed buoy and SeaStation cages are not included on the figure. This drawing is not to scale.

A monitoring buoy that included wave measuring accelerometers, a near surface current meter and an upward looking Acoustic Doppler Current Profiler (ADCP) was also deployed during the same time period to the southeast of the cage and mooring system (also shown on Figure 4). The intent was to measure wave and current forcing at the site and the corresponding attachment line

tensions. The data sets were used for comparison with numerical model results. This section describes the specific instrumentation details. It also includes a description of other data sets obtained from nearby meteorological stations and weather buoys that were also used to assess the environmental conditions at the OOA site while the cage was deployed.

3.2. Monitoring Buoy Details

As part of a large Open Ocean Aquaculture program at the University of New Hampshire (http://ooa.unh.edu), a permanent monitoring buoy has been deployed at the site for several years for measuring physical and environmental parameters associated with exposed aquaculture operations. The buoy system is heavily instrumented and uniquely moored. A system schematic is shown on Figure 5 with design details provided in Irish et al. (2004). In this study, data sets from the wave measuring system and the near surface current meter were utilized to understand the environmental forcing characteristics interacting with the deployed cage system.

The wave measuring system on the buoy consists of a three-axis accelerometer package connected to the data acquisition system in the hull of the buoy. Measurements made by Ahern (2002), show that within the wave frequency range, the buoy has nearly a one-to-one heave response to wave amplitude relatetionship, therefore providing an effective platform for measuring surface elevations. The wave measurement system is used to find the energy based significant wave height (H_{mo}) and the dominant wave period (T_p).

The energy based significant wave height (H_{mo}) is obtained by first finding the spectral representation of the data using fast Fourier transforms. In the process, eleven sections of the time series are ensemble averaged between of the frequencies of 0.02 to 5 Hz. In the frequency domain, low frequency noise is “subtracted” from the spectral estimates by removing the trend. The displacement spectrum is obtained by frequency integration. Assuming that each spectrum is narrow banded and follows a Rayleigh distribution, the H_{mo} can be estimated as four times the square root of the variance, where the variance is the area under the spectral curve. The dominant wave period is taken as the inverse of the wave frequency where the highest energy occurs.

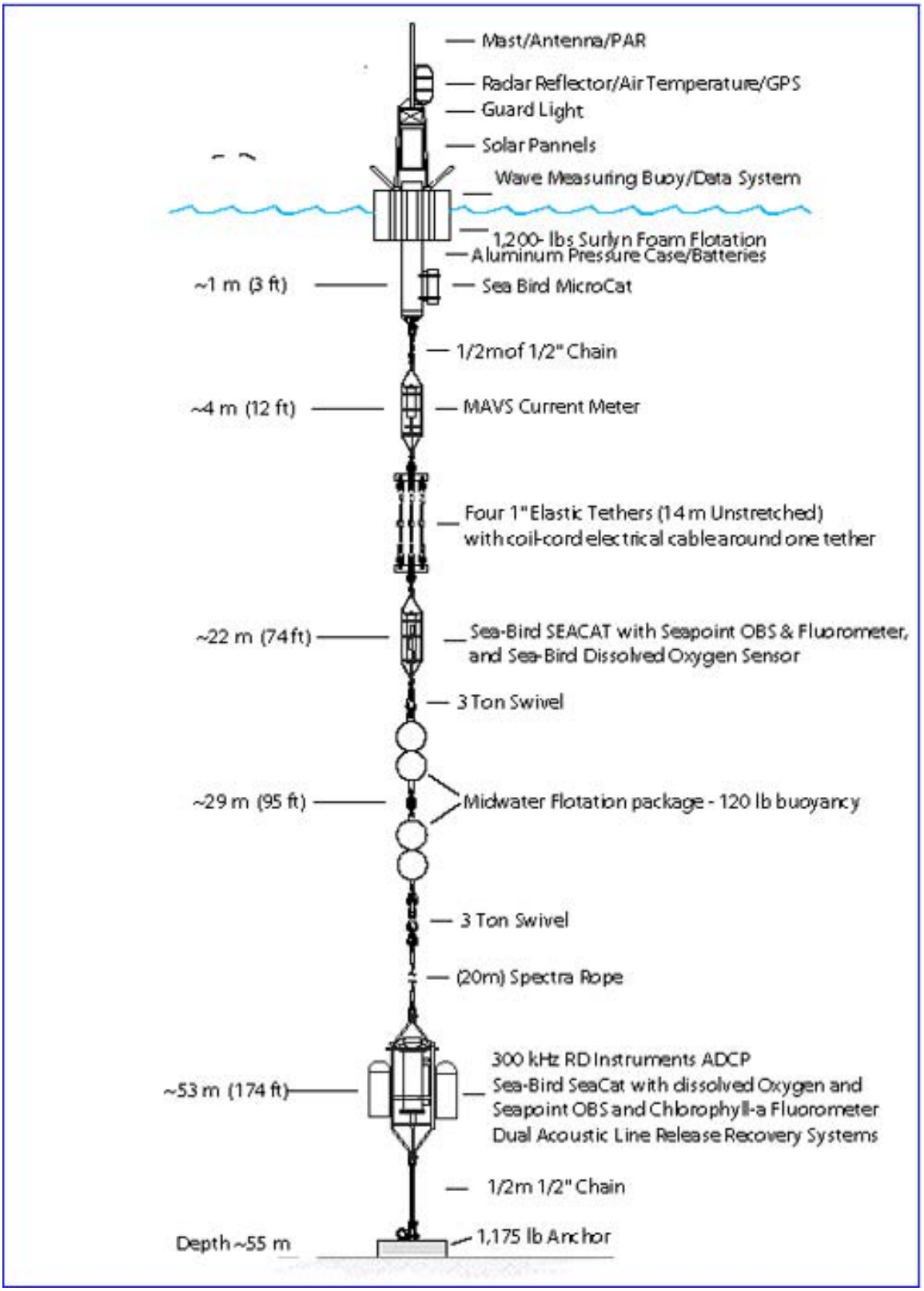

Figure 5: Wave and current data sets obtained from the monitoring buoy located at site.

Near surface velocities were made with a current meter also attached to the monitoring buoy. As shown on Figure 5, a MAVS (www.nobska.net) current meter is located at an approximate depth of 4 meters. The MAVS current meter uses differential travel time measurements to estimate velocity. The MAVS also records temperature, tilt and orientation, and provided velocity in earth coordinates. The instrument was set to record one minute averages (sampling at 1 Hz) every 15 minutes. Velocities throughout the water column were measured with the ADCP mounted at the bottom of the instrumentation platform and pointing up (Figure 5). The ADCP was set to record current velocities at 2 meter depth bins, performing 600 pings at 1.8 seconds to produce a sampling interval of 18 minutes and 54 seconds. An average over the interval is recorded.

3.3. Load Cells

To measure cage attachment line tensions, two in-line load cells were deployed as part of the mooring system (Figure 6). The load cells were designed for underwater aquaculture operations by Sensing Systems Corporation of New Bedford, MA and were constructed with a working tension range of 0 to 133 kN, but survivable to 267 kN. The load cells incorporate an internal amplifier for the strain gauges so that a 0 to 2.5 volt signal sent through the Impulse underwater connector would be compatible with the Persistor recorder, and the higher voltage (rather than bridge voltages) would be less affected by connector resistance effects. The load cells were designed to be insensitive to torque that would be applied by standard ropes (e.g. three-stranded) in the mooring system under varying tension and have been used as part of other marine aquaculture studies (see Fredriksson et al 2003, and Fredriksson et al 2007b). The instruments were set to record for 20 minutes every hour, sampling at 5 Hz.

The load cells and recorders were calibrated at the Woods Hole Oceanographic Institution using a Baldwin Model 60-SC Universal Testing Machine with Admet digital readout and calibrated yearly by American Calibration and Testing. Least square regressions were fit to the calibration data, compared with the pre-deployment Sensing Systems calibrations and pre-and post-deployment zeros, and the most consistent results used to normalize the data.

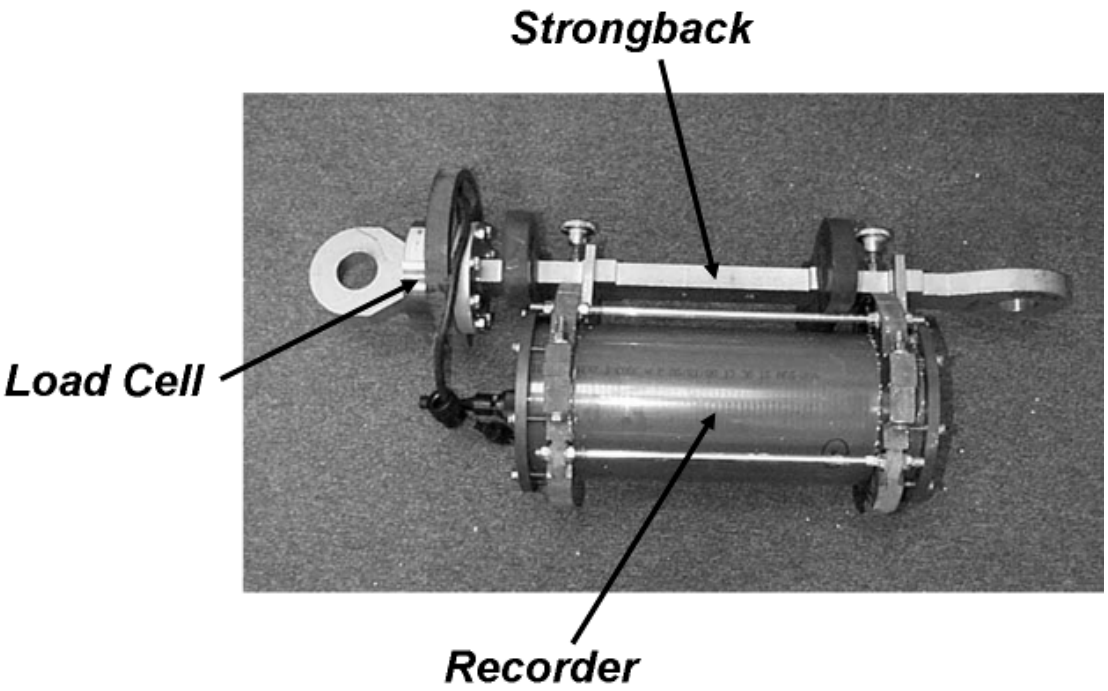

Figure 6: The load cell and strong-back with diver serviceable recorder assembly as deployed at the site.

3.4. National Data Buoy Center – Isles of Shoals

Since the acceleration data sets from the aquaculture buoy were not processed to obtained wave direction, wind information from the National Data Buoy Center (NDBC) Isles of Shoals site (Station IOSN3) was investigated to infer wave direction. Station IOSN3 is located at 42.97N Latitude and 70.62W longitude, approximately 2 km north of the aquaculture site. Most of the waves used in the analysis were likely wind generated, so wind direction was assumed to be similar to the wave direction. The NDBC website is at www.ndbc.noaa.gov.

3.5. National Data Buoy Center – Buoy B0102

Additional environmental data sets were obtained from an oceanographic buoy at NDBC station 44030 located at 43.18N latitude and 70.43W longitude. This buoy is maintained by the Gulf of Maine Ocean Observing System (Buoy B0102), but data sets can be found at the same NDBC website as Station 44030. Wind speed, wind direction and wave height data sets from Station 44030 were used to assess environmental conditions during times when the OOA wave accelerometers were not providing information.

4. Field Measurement Results

4.1. Surface Waves

Surface wave characteristics were inferred from accelerometers mounted on the wave following buoy deployed to the southeast of the mooring system. Data sets were acquired from this system between 08/14/2006 and 08/31/2006. The wave acceleration processing technique was used to obtain the top 25 waves and is provided on Table C.1 (Appendix C). Since wave measurements were not collected from the OOA buoy for the entire deployment period, wave information was also obtained from NDBC station 44030. Station 44030 is located approximately 30 km from the OOA buoy. To assess the similarities between wave conditions at each site, the H_{mo} from Station 44030 was compared with each of the highest wave conditions measured with the OOA buoy. The resulting data set, showing the similarities, is also shown on Table C.1.

4.2. Ocean Currents

The MAVS current meter was deployed from 08/15/2006 to 11/03/2006. The MAVS was attached to the wave rider buoy, located to the SE of the grid, approximately 4 m below the water surface (Section 3.1). The data was processed into east- and north-going components after applying a compass declination correction. The results are shown on Figure D.1. The data set was examined for the highest current velocity magnitudes. The top 25 current speeds are provided on Table D.1 along with each of the east- and north-going components and the time when the event occurred. The maximum measured current speed during the deployment period was 50.3 cm/s and occurred on 08/21/2006 at 1030 UTC. Note that 21 of the 25 top speeds are traveling in the northeast direction (from the southwest). The average current speed during the deployment was 13 cm/s. Since the load cells were deployed on the eastern attachment lines, examining the currents coming from the east-going direction will likely provide strong load cells measurements useful for model comparison. Therefore, the current velocity data set was then processed for the highest 25 events with a negative east-going value. The results are provided in Table D.2.

Since the ADCP collects such large amounts of data, general processing was not performed. Instead case study options were investigated using the MAVS data set. Once a specific event was identified, the ADCP profile was examined for that situation.

4.3. Load Cell Measurements

The NE load cell collected data from 07/12/2006 at 1800 UTC to 09/30/2006 at 0600 UTC. The load cell data was processed using the sensitivity of 30.38 kN/volt (6831.3 lbf/volt) and offset of 0.0509 volts measured during the calibration process. The maximum, average and standard deviation from each 20 minute time series data set are shown on Figure E.1. To examine the data set for likely load case candidates, the measurement results were sorted and the highest tension events were obtained. The results are provided in Table E.1. The highest force measured in the northeast y-line during this deployment period was 15,033 N (3380 lbf) on 07/23/2006 at 1300 UTC.

The SE load cell collected data from 07/12/2006 at 1800 UTC to 10/27/2006 at 0300 UTC. The load cell was processed using sensitivity and offset values of 29.49 kN/volt (6629.4 lbf/volt) and 0.0716 volts respectively. The maximum, average and standard deviation from each 20 minute time series data set are shown on Figure E.2. To examine the data set for likely load case candidates, the measurement results were sorted and the highest tension events were obtained. The results are provided in Table E.2. The highest force measured in the southeast attachment line during this deployment period was 14,231 N (3199 lbf) on 10/26/2006 at 0600 UTC.

4.4. NDBC Data Sets

Wind speed and direction information was obtained from the NDBC stations IOSN3 and 44030. The data downloaded from the NDBC website is provided in Appendix F. The wind speed and direction from Station IOSN3 for July through October is shown on Figure F.1. The wind speed and direction as well as the significant wave height information from Station 44030 are shown on Figure F.2. Note that wave data are not available from Station IOSN3 since it is a land-based meteorological station.

5. Field Measurement Considerations for Model Load Cases

5.1. Load Case Considerations

The SBIR cage system was deployed at the open ocean site from July to November 2006. As previously described, one of the purposes of the field measurement program was to obtain a combination of data sets that could be used as input to the numerical model (waves and currents) so that calculations could be made and compared with measured attachment line tensions. During the deployment period not all of the instruments returned the same amount of information

to characterize all of the forcing and loading events (though many candidate load cases can be obtained for numerical model investigation). Several conditions for which data sets were available were considered for use with the Aqua-FE model. For example, data sets for the following field conditions were examined:

1. Relatively high waves measured at the site
2. Highest measured value from the NE load cell
3. Highest measured value from the SE load cell
4. Strongest current measured at the site
5. Strongest west-going current measured at the site
6. Largest wave condition measured during cage deployment

From the load case analysis, two conditions were chosen to (1) validate the numerical model approach and to (2) evaluate qualitatively the performance of the system under extreme conditions. The data sets obtained on 08/28/06 at 1500 UTC and 10/29/06 at 0000 UTC were used for comparison and extreme condition performance purposes, respectively. The specific data from these time periods are further described in the following sections.

5.2. Model Comparison Load Case

The first step in the model validation process was to identify a comprehensive data set for model input parameters and resulting output comparisons. One of the highest wave conditions for which data was available at the OOA site, occurred at 08/28/2006 at 1500 UTC. At this time, the waves were generally coming from the north and the NE measured tensions were substantially higher than those from SE. Also on this date, the MAVS current meter, located on the instrumentation buoy, recorded east- and north-going velocity components at 1500 UTC. The results are provided on Table 1. Also provided on Table 1 are the current velocity components before and after 1500 UTC to show evidence of nearly steady-state conditions.

Table 1: Velocity measurements obtained from the MAVS current meter

Load Case Date	Time (UTC)	East-going (m/s)	North-going (m/s)
08/28/2006	1445	-0.161	-0.102
	1500	-0.150	-0.080
	1515	-0.198	-0.052
	1530	-0.201	0.039

At the same time that the current velocities were measured, wave accelerations were also being acquired. Using the processing techniques described in Section 3.2, a wave spectral representation was obtained (Figure 7). As shown on the Figure, it was estimated that the waves had an H_{mo} and T_p of 1.3 m and 7.88 seconds, respectively.

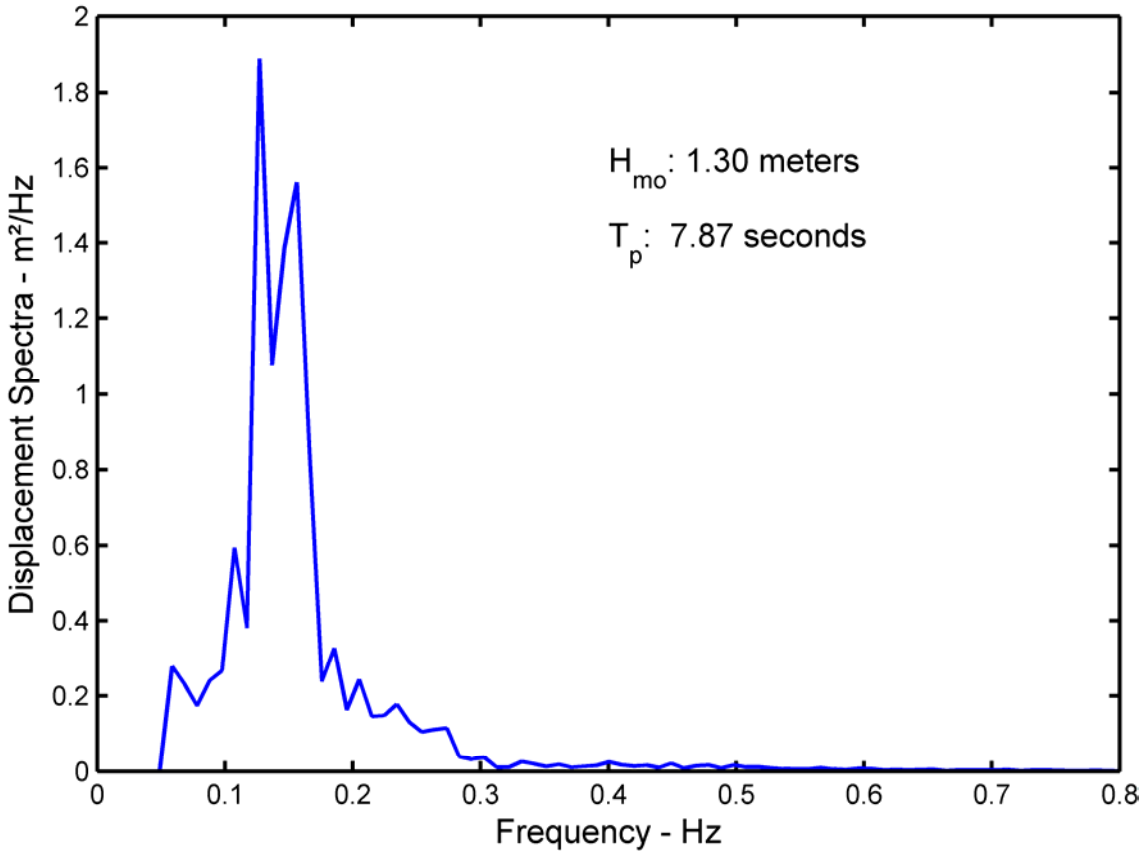

Figure 7: The wave spectral characteristics recorded on 08/28/06 at 1500 UTC from the instrumentation buoy at the OOA site.

The wave information shown on Figure 7, however, does not indicate the direction that the waves were coming from. The directional information is critical to the forcing input of the numerical model so that appropriate tensions in the attachment lines are calculated. It is likely that the waves are predominantly wind driven so anemometer data sets from the NDBC station I0SN3 were examined to determine wind direction and therefore infer the direction of the waves. The wind speed and direction was obtained from the Isles of Shoals site for 0.5 hours before and after 1500 UTC on 08/28/2006. The information is provided in Table 2.

Table 2: Wind speed and direction measurements from the Isles of Shoals

Load Case Date	Time (UTC)	Direction (Degrees)	Wind Speed (m/s – Ave)
	1430	325	5.1
08/28/2006	1440	331	4.9
	1450	335	4.8
	1500	341	4.4
	1510	346	4.7
	1520	348	4.7
	1530	344	4.0

In addition to the current velocity, surface waves and wind information, load cell data sets were also acquired during the same time. As shown on Figure 4, load cells were connected to the attachment lines on the eastern side of the cage, one to the NE and one to the SE. Time series results from 1500 - 1520 UTC for each of the load cells is shown on Figure 8, while the basic statistics associated with each the time series is provided in Table 3.

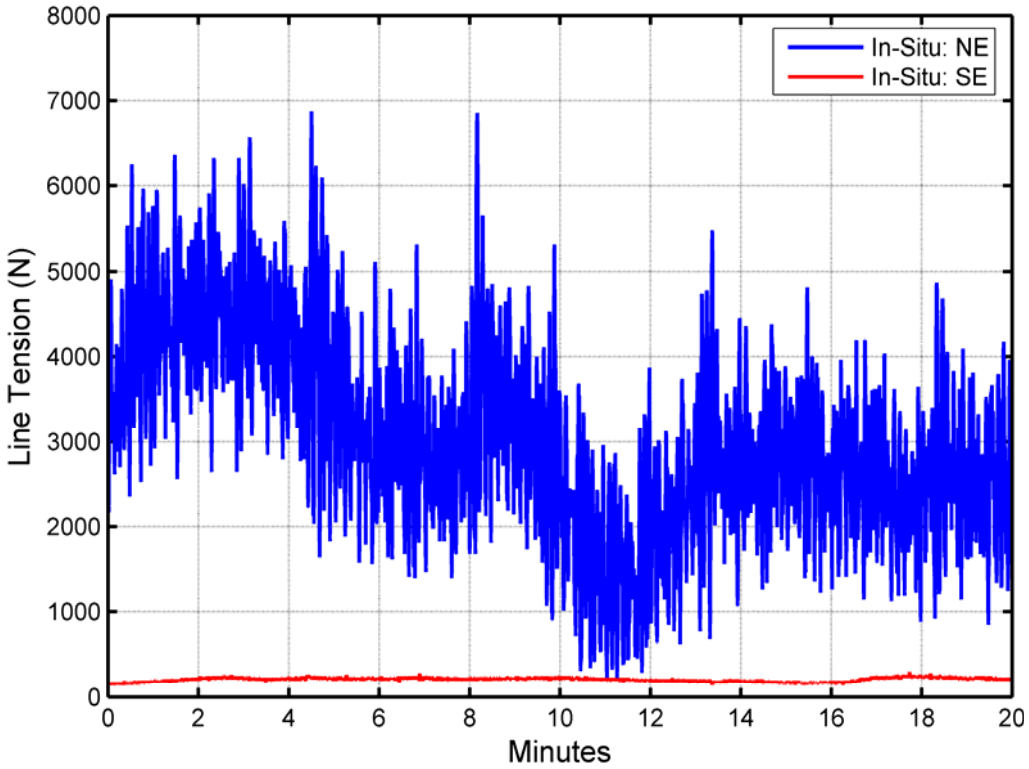

Figure 8: Time series data from the NE and SE load cells from 1500 – 1520 UTC on 08/28/2006.

Table 3: The basic statistics from each of the load cells from 1500 – 1520 UTC on 08/28/2006

08/28/2006 1500 - 1520 UTC	NE (N)	SE (N)
Maximum	6873	300
Minimum	197	138
Mean	3011	207
Standard Deviation	1155	24

This comprehensive data set acquired at the OOA site was used with the Aqua-FE model. The current velocity and wave characteristics were incorporated as input to the model and the resulting calculated tensions compared with the load cell measured values

5.3. Extreme Condition Performance Load Case

In addition to the data used for model validation, an additional data set was obtained from the cage deployment period that represented a more extreme condition. The most energetic open ocean condition during the deployment period occurred on 10/29/2006 at 0000 UTC. At this time, not all of the instruments were functioning. However a collection of data sets was gathered from the region to assess the overall environmental climate. The available data sets were obtained from (1) the MAVS current meter at the site, (2) wind speed, direction and gust from NDBC station I0SN3, (3) wind speed, direction and gust from NDBC station 44030 and (4) the wave characteristics (H_{mo} and T_p) from NDBC station 44030.

The NDBC meteorological site IOSN3 provides continuous wind data at 10 minute intervals. During this time, velocity measurements were acquired from the OOA site. Wave accelerations were not obtained at the OOA site on 10/26/2006. Therefore, wave characteristics at the OOA site were estimated to be similar to those at the NDBC 44030 Buoy (see Table C.1). The NDBC station 44030 recorded significant wave heights of 5.7 meters with dominant wave period of 11 seconds. Also, if the wind speeds, fetch and duration between the two sites are similar, so should the deep water waves. However, it has been indicated that the wave conditions at Station 44030 are similar to that at the OOA site (see Table C.1). Furthermore, if the waves are similar, so may the wind speeds. A comparison of wind speed and direction from Stations I0SN3 and 44030 is provided in Table 4 showing reasonable agreement.

Table 4: Wind speed and direction measurements from the Isles of Shoals and NDBC station 44030 on 10/28/06 at 1130 UTC to 10/29/2006 0030 UTC. Also included on the Table

	Time (UTC)	Direction (Degrees)	Wind Speed (m/s – Ave)	Wind Gust (m/s)
	1130	161	15.9	-
IOSN3	1140	165	13.8	-
	1150	165	12.7	-
10/29/06	0000	165	12.1	-
	0010	170	11.3	-
	0020	172	10.5	-
	0030	177	10.5	-
	2300	161	17.3	12.6
IOSN3	0000	167	11.9	12.6
10/29/06	0100	203	9.7	10.2
Average		**177**	**12.7**	**11.8**
	2300	160	13.0	17.0
44030	0000	170	11.0	14.0
10/29/06	0100	180	8.0	10.0
Average		**170**	**10.7**	**13.7**

In addition to the waves, ocean current information was also required for input to the numerical model. Fortunately, the MAVS current meter was operational on 10/29/2006. The east- and north-going components (compass corrected) are provided on Table 5 from 1145 (on 10/28/2006) to 0030.

Table 5: Velocity measurements obtained from the MAVS current meter

Load Case Date	Time (UTC)	East-going (m/s)	North-going (m/s)
	1145	15.58	5.91
10/29/2006	0000	13.01	4.36
	0015	15.66	1.57
	0030	10.55	2.01

6. Finite Element Model

6.1. Theoretical Review

Numerical model simulations were performed using a FEM computer program. The program employs a modified version of Morison equation (Morison et al., 1950) to calculate hydrodynamic forces on structural, truss-like elements. Following Haritos and He (1992), Morison equation is modified to account for the relative motion between the structural element and the surrounding fluid. The fluid force per unit length is represented as

$$\mathbf{f} = C_1\mathbf{V}_{Rn} + C_2\mathbf{V}_{Rt} + C_3\dot{\mathbf{V}}_n + C_4\dot{\mathbf{V}}_{Rn}, \qquad (1)$$

where $\mathbf{V}_{Rn}$ and $\mathbf{V}_{Rt}$ are the normal and tangential components of the fluid velocity relative to the structural element, $\dot{\mathbf{V}}_n$ is the normal component of total fluid acceleration and $\dot{\mathbf{V}}_{Rn}$ is the normal component of fluid acceleration relative to the structural element. The coefficients in equation (6) above are given by $C_1 = \frac{1}{2}\rho_w D C_n V_{Rn}$, $C_2 = C_t$, $C_3 = \rho_w A$ and $C_4 = \rho_w A C_a$, where D and A are the diameter and the cross-sectional area of the element in the deformed configuration, ρ_w is the water density, C_n and C_t are the normal and tangential drag coefficients. Coefficients C_3 and C_4 represent the inertial force components due to the fluid acceleration where C_a is the added mass coefficient. Note that C_n and C_a are dimensionless, while C_t has the dimension of viscosity.

The numerical procedure calculates C_n and C_t, using a method described by Choo and Casarella (1971) that updates the drag coefficients based on the Reynolds number (Re_n) as follows

$$C_n = \begin{cases} \dfrac{8\pi}{\mathrm{Re}_n\, s}\left(1 - 0.87 s^{-2}\right) & \left(0 < \mathrm{Re}_n \le 1\right), \\ 1.45 + 8.55\,\mathrm{Re}_n^{-0.90} & \left(1 < \mathrm{Re}_n \le 30\right), \\ 1.1 + 4\,\mathrm{Re}_n^{-0.50} & \left(30 < \mathrm{Re}_n \le 10^5\right) \end{cases} \qquad (2)$$

$$C_t = \pi\mu\left(0.55\,\mathrm{Re}_n^{1/2} + 0.084\,\mathrm{Re}_n^{2/3}\right) \qquad (3)$$

where $\mathrm{Re}_n = \rho_w D V_{Rn}/\mu$, $s = -0.077215665 + \ln\left(8/\mathrm{Re}_n\right)$ and μ is the water viscosity. The coefficients C_1, C_2, C_3 and C_4 can be calculated assuming that the structural elements are smooth

circular cylinders or modified to represent the hydrodynamics of other element types such as non-cylindrical buoys or nets. For example, Tsukrov et al. (2003) used this approach to develop the consistent net element.

The model also incorporates the buoyancy, weight, inertia and elastic forces of the element. Introducing linear finite elements with two nodes having three degrees of freedom (nodal displacements) each, the forces are discretized using a shape function matrix so that the forcing components on each element can be integrated over the length of the element. The standard finite element discretization of the structural system in a moving fluid environment results in the following system of differential equations,

$$(\mathbf{M}+\mathbf{m})\ddot{\mathbf{q}}+\mathbf{C}\dot{\mathbf{q}}+\mathbf{K}\mathbf{q}=\mathbf{R}+\mathbf{H} \qquad (4)$$

where $\mathbf{q}$ is the (time dependent) vector of nodal displacements, $\mathbf{M}$ is the time independent consistent mass matrix, $\mathbf{m}$ is the virtual mass matrix, $\mathbf{C}$ the damping matrix (due to fluid drag), $\mathbf{K}$ is the global stiffness matrix (which can be expanded into a tangent stiffness matrix and internal force vector), $\mathbf{R}$ is the equivalent nodal force vector due to gravity and buoyancy forces and $\mathbf{H}$ is the equivalent nodal force vector due to wave and current loads.

In the model, equations (4) are discretized in time and integrated using the Newmark-Beta method. The Newton-Raphson iteration scheme is employed to find nodal displacements at every time step from which velocities, accelerations and stresses are obtained. The model also includes a non-linear Lagrangian formulation to account for large displacements of structural elements.

6.2. Geometric and Material Properties

The numerical model requires the geometric and material properties of the fish cages and mooring system. The parameters include the mass density, Young's Modulus and cross sectional area of each element component. The geometric and material properties for the SBIR cage are provided in Table 6, from which the system was built in the model. The model included not only the SBIR cage system, but also the SS600 and SS3000 cages as described in Section 2. At the site, the SS600 and SS3000 were deployed in a submerged configuration and therefore were modeled in the same manner. It also should be noted that the SS600 was deployed without nets.

The modeling details of these fish cages are provided in Fredriksson et al. (2004). Another component of the deployed system, and also modeled, was an automated feeding buoy attached to the SS3000 fish cage. The construction and modeling details for the feeding buoy are provided in Fullerton et al. (2004). Using the geometric and material properties of the SBIR, SS600 and SS3000 fish cages, along with the automated feeding buoy, a comprehensive model was built with the Aqua-FE program. The entire model is shown on Figure 9.

Table 6: The cage component geometric and material properties used in the numerical model simulations

Component	Density (kg/m^3)	Modulus of Elasticity (Pa)	Cross – Sectional Area (m^2)
Outer Rim	324.4	1.172×10^{9}	3.8×10^{-2}
Inner Rim	329.0	1.172×10^{9}	3.8×10^{-2}
Net chamber	1025	2.0×10^{10}	2.835×10^{-6}
Stays	963.5	9.948×10^{8}	1.267×10^{-4}
Lower Rim	1043	1.172×10^{9}	3.8×10^{-2}
Bridle	963.5	9.948×10^{8}	1.267×10^{-4}
Airlift	428.0	2.00×10^{11}	4.04×10^{-1}
Ballast Line	963.5	1.032×10^{9}	7.917×10^{-4}
Ballast Chain	7849	2.00×10^{11}	6.067×10^{-3}
Ballast Chain Clump	7849	2.00×10^{11}	1.80×10^{-3}

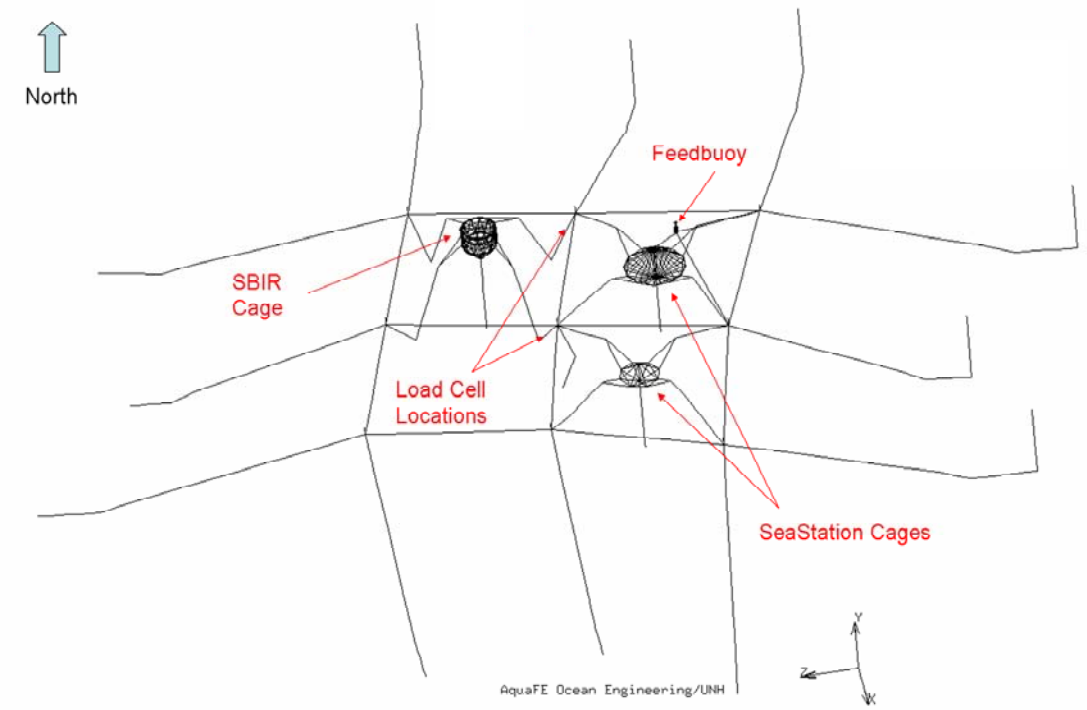

Figure 9: The constructed cage and submerged mooring in Aqua-FE. The currents and waves were applied to the model and the tensions in the eastern y-lines were recorded.

6.3. Forcing Input Parameters

6.3.1. Model input for conditions that occurred on 8/28/2006

The forcing input parameters to the Aqua-FE model included a combination of waves and currents. The surface elevation time series was generated using the spectral information shown on Figure 7 assuming a linear superposition of the wave frequency components,

$$\eta(t) = \sum_{i=1}^{n} a_i \cos(\omega_i t + \phi_i). \qquad (5)$$

In equation (5), a_i, ω_i and ϕ_i are the wave amplitudes, radian frequencies and phases, respectively. The spectral information on Figure 7 was decomposed into 91 amplitudes, frequencies and phases and superimposed to create a time series according to equation (5). The result is shown on Figure 10. The waves were orientated at an angle of 345 degrees (True).

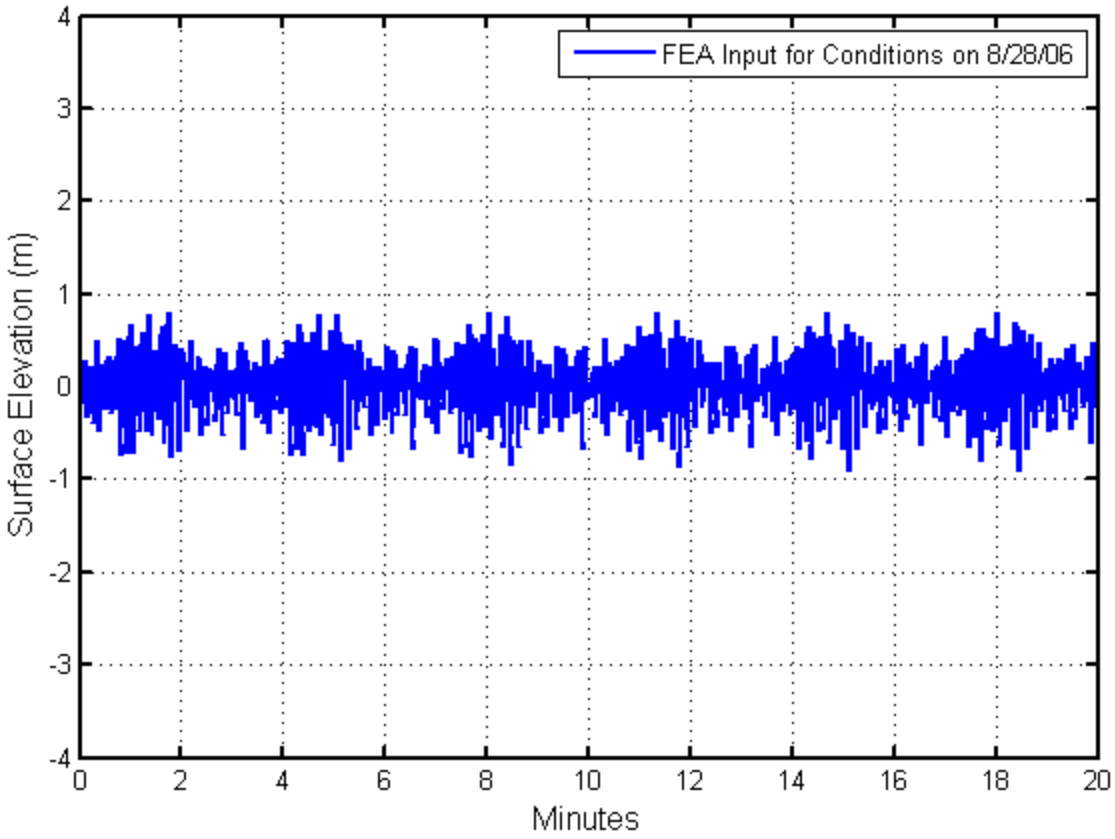

Figure 10: The FEM surface elevation time series input.

The current velocity input to the numerical model consisted of a combination of data from the MAVS and ADCP instruments collected on 8/28/2006 between 1500 and 1520. As discussed in Section 3.2, the MAVS current meter collected one minute averages at 1500 and 1515 at a depth of approximately 4 meters. The ADCP data set included current profiles between 1500 and 1519. From a depth of 0 to 5 meters, however, the ADCP does not acquire information due to back scattering effects. Therefore, the MAVS data is used at the near surface. A composite profile was used for input to the Aqua-FE program. At the depth of 0 and 4 meters, the average MAVS value from 1500 and 1515 was used for each of the north- and east-going components, 6.6 and -17.4 cm/s, respectively. For the rest of the water column (depths 6 to 48 m), the average values from the ADCP were incorporated into the input profile. The composite data set is shown in Figure 11.

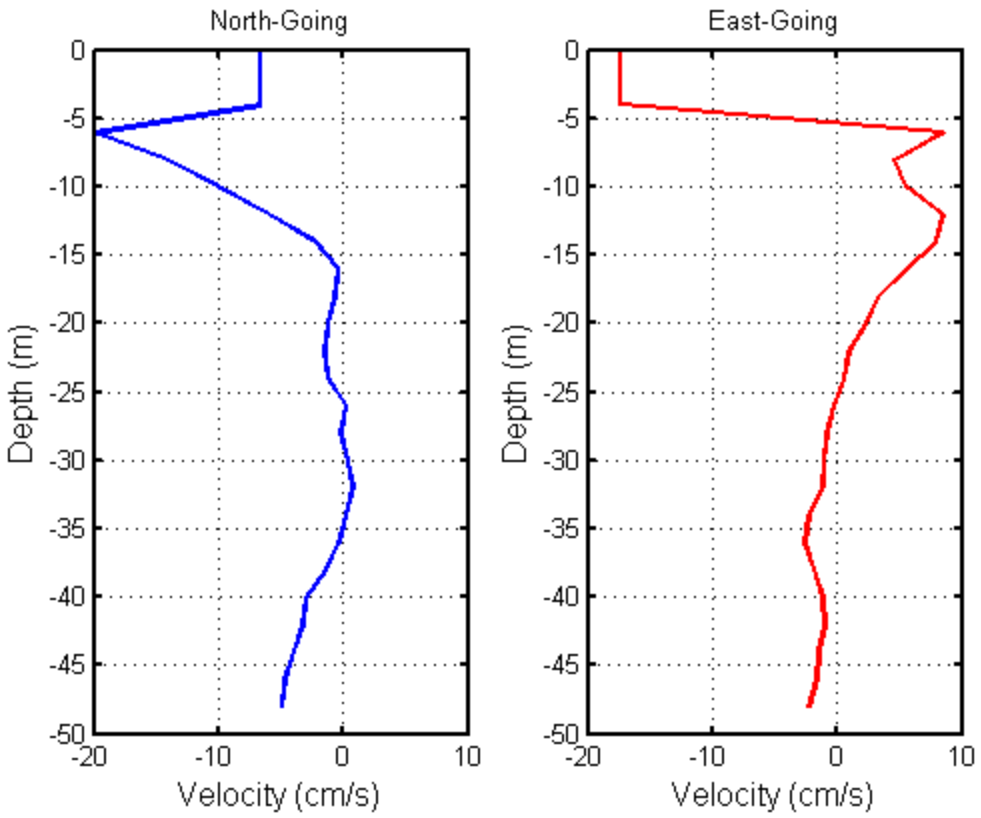

Figure 11: The composite current velocity data set included information from both the MAVS and ADCP instrument.

6.4. Results

The wave and current velocity information was entered into the Aqua-FE program and a 15 minute simulation was performed. The simulation produces stress results in the mooring system attachment lines from which forces are obtained. The force results for the NE, NW and SE attachment lines are shown in Figure 12. The basic statistics for both the in-situ and the model results are provided in Table 7. Review of the results indicate that while individual values do not appear to match, the combined load comparisons between the set of mooring attachments (e.g. both the NE and SE) show much smaller differences. This is perhaps a result of the difficulty representing the exact geometry of the deployed system and the low levels of forcing. This being said, it can be assumed that the model is working reasonably well.

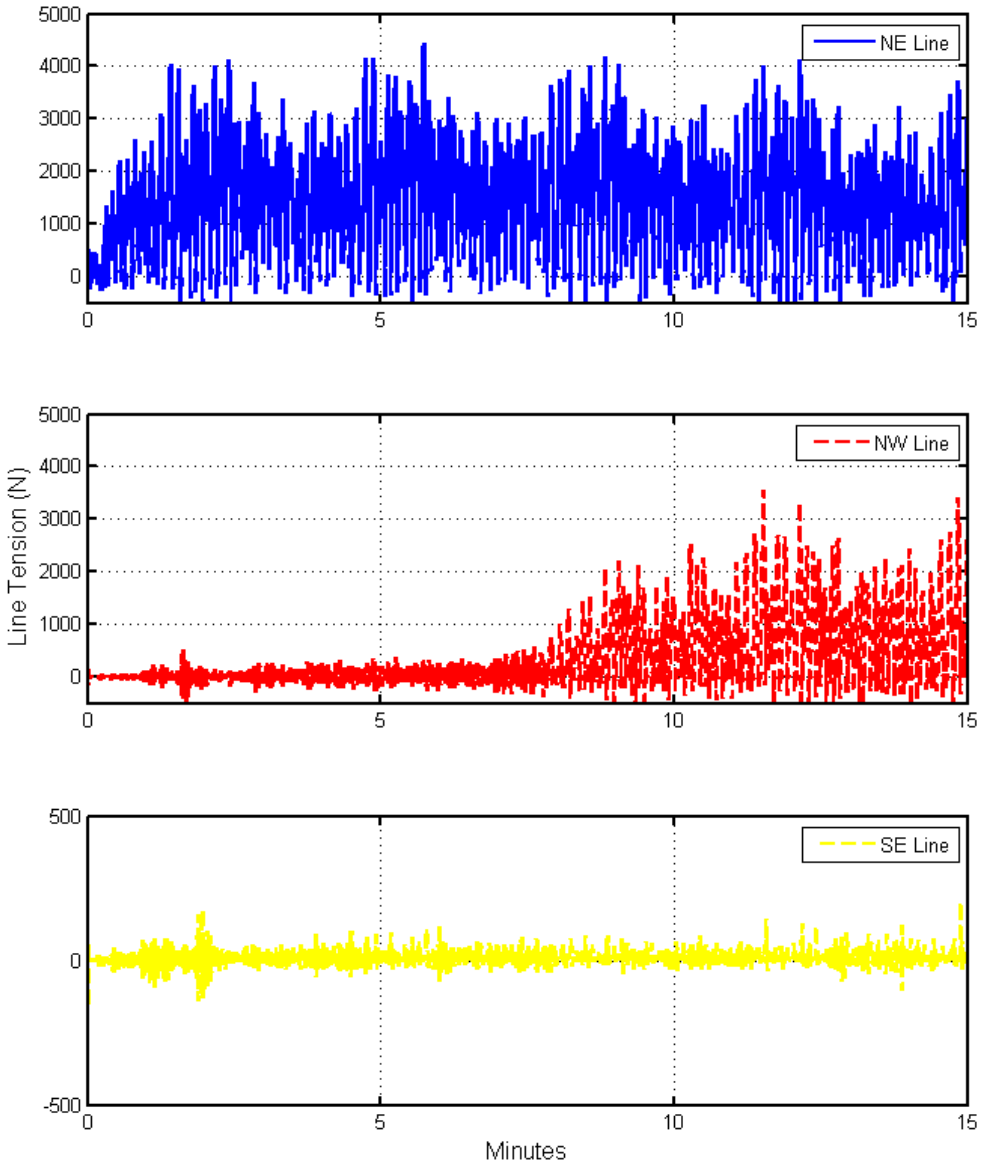

Figure 12: The results of the FEM simulation for conditions described in Section #.#.

Table 7: A comparison of in-situ and model results

08/28/2006 1505 - 1515 UTC	NE: In-Situ[1] (N)	NE: Model[2] (N)	SE: In-Situ[1] (N)	SE: Model[3] (N)
Maximum	6855	4449	282	3497
Minimum	197	-740	138	-686
Mean	2626	1384	206	711
Standard Deviation	1007	1066	19	800

[1]In-situ averages were taken between 1505 and 1515 UTC
[2]NE attachment line load averages were taken between 5 and 15 minutes of simulation
[3]SE attachment line load averages were taken between 10 and 15 minutes of simulation

7. Model results with more extreme environmental conditions

The next step in the process was to investigate the potential attachment line tensions to the SBIR cage under more extreme conditions. The system survived the entire deployment period under worse conditions than described in Section 6.3. In most cases, however, complete in-situ data sets were not available to perform a full comparative analysis. To investigate attachment line loads, environmental conditions were estimated, used as input to the numerical model and simulations performed. The calculated stresses in the attachment lines were used to estimate the potential loads on the rim of the cage.

The next step was to gather all of the available environmental data sets for a more extreme situation and as discussed in Section 5.3, conditions on 10/29/2006 were chosen. On 10/29/2006, only the H_{mo} and T_p wave characteristics were available. Therefore, wave input to the model was represented as a random sea condition using a modified version of the JONSWAP spectra described by Goda (1985),

$$S(f) = \alpha H_s^2 T_p^{-4} f^{-5} \exp\left[-1.25(T_p f)^{-4}\right] \gamma^Y, \tag{6}$$

where

$$Y = e^{\left[-(T_p f - 1)^2 / 2\sigma^2\right]} \tag{7}$$

$$\alpha = \frac{0.0624}{0.23 + 0.0336\gamma - 0.185(1.9 + \gamma)^{-1}}, \tag{8}$$

and

$$\sigma = \begin{cases} \sigma_a : f \le f_p \\ \sigma_b : f \ge f_p \end{cases}, \tag{9}$$

and f_p is the frequency at the spectral peak ($1/T_p$). Parameters γ and σ are used to adjust the height and width of the peak of the curve, respectively. In equation (6), a value of 5.7 meters, obtained from a Station 44030 data set (Section 5.3) was used for H_s. The dominant wave period (T_p), equal to 11 seconds, was used in equations (6), (7) and (9). Fitting parameters γ, σ_a and σ_b with values of 3.3, 0.09 and 0.07, respectively were applied in equations (8) and (9). The resulting spectrum was decomposed into a time series using equation (5) and applied in the FEA model. The time series is shown in Figure 10b. The waves were orientated at a direction of 168

degrees true. Current velocity components were superimposed with the waves having an east-going component of 0.0436 m/s and a north-going component of -0.1301 m/s.

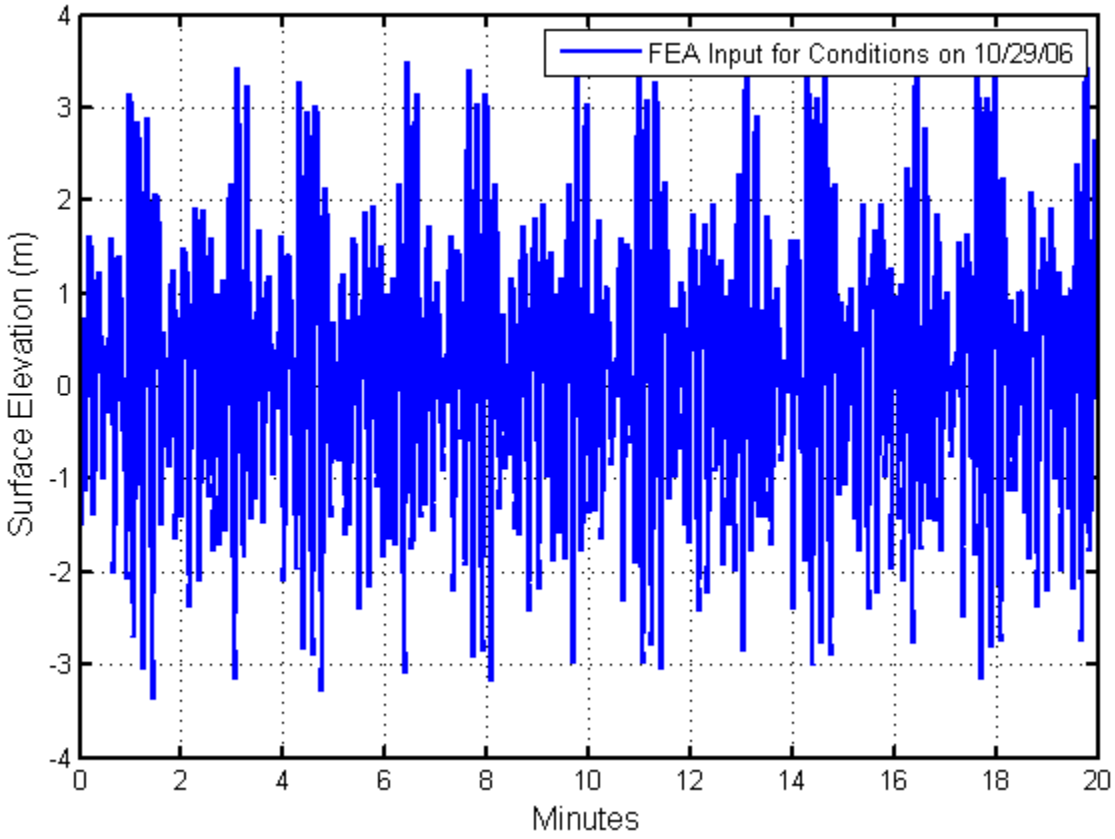

Figure 13: The wave information input to the model for 10/29/2006.

The numerical model was then used with the described input parameters and a simulation was performed for duration 15 minutes. The resulting time series line tension results are shown on Figure 12. The maximum minimum, mean and standard deviation from this data set, for steady conditions, is provided in Table 8.

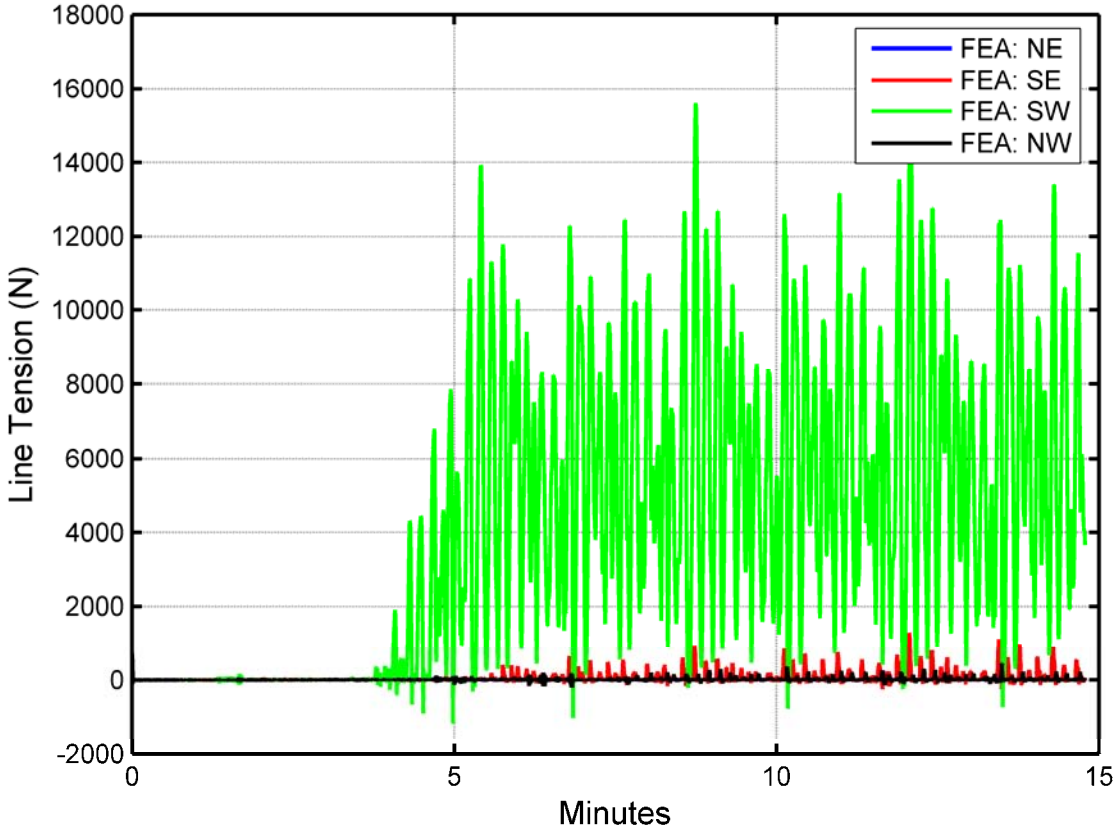

Figure 14: The line tension results using the Aqua-FE model for the conditions that occurred on 10/29/2006 at 0000 UTC

Table 8: The basic statistics obtained from the Aqua-FE model for 10/29/2006

10/29/2006 0000 - 0020 UTC	NE (N)	SE (N)	NW (N)	SW (N)
Maximum	90.52	1291	452.9	16072
Minimum	-40.81	-252.2	-207.4	-1005
Mean	9.58	82.52	21.25	5742
Standard Deviation	12.36	21.27	49.89	3354

8. Conclusion

The environmental conditions that occurred on 10/29/2006 can be considered relatively extreme. Maximum attachment loads were about 16000 N. Inspection of the cage after the deployment period showed no major structural failures. This indicates that size of the pipe chosen and the design of the custom made connection components may be suitable for application in this environment. Furthermore, if even more extreme design conditions are investigated, the Aqua-

FE model could be applied to estimate the resulting attachment line loads. Then the structural modeling approaches similar to those described in Fredriksson et al 2007a can be applied if cage modifications are considered.

9. Acknowledgements

The project was funded as a subcontract to JPS Industries on a project funded through the National Oceanic and Atmospheric Administration, SBIR program, contract number DG133R05CN1247.

10. References

Ahern, J. (2002). Validation of wave measurement buoy. Master's Degree Thesis submitted in partial requirement for the Ocean Engineering degree program. University of New Hampshire, Durham, NH. 101 p.

Choo,Y.I. and Casarella, M.J., (1971). Hydrodynamic resistance of towed cables. J. Hydro. 126-131.

Fredriksson, D.W., M.J. Palczynski, M.R. Swift, J.D. Irish and B. Celikkol. (2003). Fluid dynamic drag of a central spar cage in C.J. Bridger and B.A. Costa-Pierce, editors. Open Ocean Aquaculture: From Research to Commercial Reality. The World Aquaculture Society, Baton Rouge, Louisiana, United States. pp 151-168.

Fredriksson, D.W., J. DeCew, M.R. Swift, I. Tsukrov, M.D. Chambers, B. Celikkol. 2004. The design and analysis of a four-cage grid mooring for open ocean aquaculture. Aqua Eng. Vol 32, pp 77-94.

Fredriksson, D.W., DeCew, J.C., and I. Tsukrov. (2007a). Development of structural modeling techniques for evaluating HDPE plastic net pens used in marine aquaculture. Ocean Eng. (in press).

Fredriksson, D.W., DeCew, J.C., Tsukrov I., Swift, M.R., and J.D. Irish. (2007b). Development of large fish farm numerical modeling techniques with in-situ mooring tension comparisons. Aqua Eng. Vol 36, pp 137-148.

Fullerton, B., Swift, M.R., Boduch, S., Eroshkin, O., and G. Rice. (2004). Design and analysis of an automated buoy for submerged cages. Aqua Eng. Vol 32, pp 95-111.

Goda, Y. (1985). Random Seas and the Design of Maritime Structures. World Scientific Publishing Company, New Jersey. 443 p.

Haritos, N and D. T. He. (1992). "Modelling the response of cable elements in an ocean environment". Fin. Elem. in Analysis and Des. vol 19, pp. 19-32.

Irish, J.D., Paul, W., and D.M. Wyman. (2005). The Determination of the elastic modulus of rubber tether moorings and their use in coastal moorings. Woods Hole Oceanographic Institution, Technical Report WHOI-2005-10. p. 42.

Irish, J.D., Fredriksson, D.W., and S. Boduch (2004). Environmental monitoring buoy and mooring with telemetry. Sea Tech. May 2004. pp. 14-19.

Morison, J.R., J.W. Johnson, M.P. O'Brien and S.A. Schaaf,, (1950) "The forces exerted by surface waves on piles". Petroleum Transactions, American Inst. of Mining Eng. Pp. 149-157.

Paul, W. (2004). Hose elements for buoy moorings: design, fabrication and mechanical properties. Woods Hole Oceanographic Institution Technical Report, WHOI-2004-06. 16 p.

Santamaria, J., Monahan, C., Scott, J., Fredriksson, D., Celikkol, B., and J. DeCew. (2007). SBIR Progress Report for the period between September 1, 2006 and March 1, 2007. Project Title: Development of a submersible fish cage for open ocean aquaculture. 15 pp.

Santamaria, J., Monahan, C., Scott, J., Fredriksson, D., Celikkol, B., and J. DeCew. (2006a). SBIR Progress Report for the period between February 1, 2006 to September 1, 2006. Project Title: Development of a submersible fish cage for open ocean aquaculture. 10 pp.

Santamaria, J., Monahan, C., Scott, J., Fredriksson, D., Celikkol, B., and J. DeCew. (2006b). SBIR Progress Report for the period between September 1, 2005 and February 1, 2006. Project Title: Development of a submersible fish cage for open ocean aquaculture. 10 pp.

Tsukrov, I., O. Eroshkin, D.W. Fredriksson, M.R. Swift, and B. Celikkol (2003). Finite element modeling of net panels using consistent net elements. Ocean Eng. Vol 30: pp.251-270.

Tsukrov, I, Eroshkin, O., Paul, W., Celikkol, B., (2005). Numerical modeling of nonlinear elastic components of mooring systems. IEEE J. Oceanic. Eng. Vol. 30, No. 1 pp 37-46.

Appendix A: SBIR cage System Components

Table A.1: SBIR Cage System Components

Component	Parameter	Value
Upper Rim	# of sections	12
	Diameter	8.625 in
	Length	12.7 ft
	Material	HDPE w/ Aluminum fittings
Angled Stays	Diameter	½ in
	Length	24.5 ft
	Material	Polysteel
Net Chamber	Twine Diameter	0.075 in
	Mesh Length	½" square
	Material	Nylon
Lower Rim	# of sections	12
	Diameter	8.625 in
	Length	12.7 ft
	Material	HDPE w/ Aluminum fittings
Bridle	Diameter	½ in
	Length	35 ft
	Material	Polysteel
Airlift	Diameter	2.5 ft
	Length	2 m
	Material	Steel
Ballast Line	Diameter	1 in
	Length	58 ft
	Material	Double braid Nylon
Ballast Chain	Mass	2880 lb
	Length	77 ft (total)
	Material	Steel

Appendix B: Feed Hose Buoy Components

The complete description of the feed hose buoy components including the name, part and materials are provided in Table B.1. In addition to the component description, additional parts are specified as provided on Table B.2.

Table B.1: Component description for the feed hose buoy.

Assembly	Name	Part #	Description	Material
Main Weldment	Feed pipe	001-001	4" feed pipe thru buoy	Alum 6061-T6 sch 40 pipe 4"
	Deck plate	001-002	main deck plate	Alum 6061-T6 3/16" plate
	Tube Upper Flange	001-003	upper main tube flange	McMaster-Carr
	Radial Angles	001-004	main deck supports	Alum 6061-T6 2x2x1/4 angle
		NONE	mirror of part# 00-001-004	Alum 6061-T6 2x2x1/4 angle
	Radial plates	NONE	plates for end of radial angles	Alum 6061-T6 2x1/4 flat bar
	Handles	NONE	3/4 bent round bar	Alum 6061-T6 3/4" round bar
Foam	Buoy Foam	002-001	buoy floation	Softlite ionomer foam
Foam Retainer Angle	Foam Retainer Angle	003-001	used to hold foam in place	Alum 6061-T6 2x2x1/4 angle
Tower Base	Tower Top Rim	004-001	top rim of tower base	Alum 6061-T6 1-1/2x1-1/2x1/4 angle
	Leg	004-002	leg of tower base	Alum 6061-T6 1-1/2x1-1/2x1/4 angle
	Base plate	004-003	base plate for tower	Alum 6061-T6 2x1/4 flat bar
	Bar support	004-004	connection in between legs	Alum 6061-T6 1x1/4 flat bar
	Rod support	004-005	tower angle support rod	Alum 6061-T6 3/8" round bar
Light Base Plate	Light Base Plate	005-001	light mounting plate	Alum 6061-T6 1/8" plate
Tower Light Extension	Tower Rim	006-001	tower rim	Alum 6061-T6 1-1/2x3/16 flat bar
	Tower Leg	006-002	tower rim leg	Alum 6061-T6 2x1/4 flat bar
	Tower Leg Base	006-003	tower leg base plate	Alum 6061-T6 2-1/2x1/4 flat bar
Tower Mast	Tower Mast Pipe	007-001	tower mast pipe	Alum 6061-T6 sch 40 pipe 1-1/2"
	Tower Mast Legs	007-002	tower leg angles	Alum 6061-T6 1/4" plate
	Tower Mast Base	007-003	tower mast base plate	Alum 6061-T6 2-1/2x1/4 flat bar

Table B.2: Component specification for the feed hose buoy.

Aluminum stock	Material	Size/Length	Quantity	Price	Notes
4" sch 40 pipe	6061-T6	5'	1		for 1 (qty) - feed pipe
3/16" thick plate	6061-T6	24x24	1		for 1 (qty) - weldment deck plate
2"x2"x1/4" angle	6061-T6	7'	1		for 4 (qty) - retainer angles
					for 2 (qty) - foam retainer angles
2"x1/4" bar stock	6061-T6	4'	1		for 4 (qty) - 2x2x1/4 pieces (retainer angle end plate)
					for 4 (qty) - 2x3-1/2x1/4 pieces (tower base leg plates)
					for 4 (qty) - 2x6x1/4 pieces (tower extension base leg plates)
3/4" round bar	6061-T6	66"	1		for 2 (qty) - bent handles
					for 1 (qty) - tower mast bilper attachment
1-1/2x1-1/2x1/4 angle	6061-T6	12'	1		for 4 (qty) - top rim tower base
					for 4 (qty) - tower base leg
1"x1/4" bar stock	6061-T6	3'	1		for 4 (qty) - 1x9x1/4 pieces (retainer angle end plate)
3/8" round bar	6061-T6	4'	1		for 4 (qty) - tower angle supports
1/8" thick plate	6061-T6	12"x12"	1		for 1 (qty) - light base plate
1-1/2"x3/16" bar stock	6061-T6	4'	1		for 4 (qty) - tower extension plate rim
2-1/2"x1/4" bar stock	6061-T6	2'	1		for 4 (qty) - 2-1/2x2-1/2x1/4 pieces (tower extension base plate)
					for 4 (qty) - 2-1/2x2-1/2x1/4 pieces (tower mast base plate)
1-1/2" sch 40 pipe	6061-T6	3'	1		for 1 (qty) - Tower mast pipe
1/4" thick plate	6061-T6	12"x24"	1		for 1 (qty) - tower mast leg angles

Miscellaneous Items	Material	Size/Length	Quantity	Price	Notes
4" pipe slip-on flange	Alum ??	4" diam	2		Standard slip on flange
4" 90deg LD coupler	Alum ??	4" NPT	1		anodized alumimum with Type 316 SS Levers
4" Threaded pipe nipple	Alum ??	4" NPT	1		4" long 4" aluminum threaded pipe nipple
4" pipe threaded flange	Alum ??	4" diam	1		Aluminum Threaded Flange Pipe Fitting

Foam	Material	Size/Length	Quantity	Price	Notes
Softlite ionomer foam	foam	to be determined	1		main buoy floation

Appendix C: Wave Conditions during the deployment

Table C.1: The highest 25 wave conditions obtained from the buoy measurements (time is in UTC)

Date/Time	H_{mo} (m)	T_p (sec)	44030 H_{mo} (m)	44030 T_p (sec)
29-Aug 1600	1.2129	5.1200	1.4	11
30-Aug 0600	1.2173	8.5333	1.2	11
29-Aug 2000	1.2175	8.5333	1.5	11
28-Aug 0900	1.2211	6.8267	1.0	5
20-Aug 1400	1.2225	14.6286	0.9	4
28-Aug 0500	1.2238	20.4800	1.0	5
29-Aug 0200	1.2647	6.4000	1.4	6
29-Aug 0600	1.2657	5.6889	1.3	6
28-Aug 1000	1.2679	6.8267	1.2	6
28-Aug 1100	1.2980	6.4000	1.3	6
28-Aug 1500	1.3036	7.8769	1.5	6
29-Aug 1700	1.3160	10.2400	1.4	6
29-Aug 1900	1.3210	5.6889	1.6	11
29-Aug 1500	1.3276	11.3778	0.6	3
28-Aug 1400	1.3365	7.8769	1.5	8
29-Aug 1800	1.3445	10.2400	1.6	11
28-Aug 1200	1.3459	6.4000	1.3	6
29-Aug 0500	1.3729	6.4000	1.4	5
29-Aug 0300	1.4192	6.0235	1.5	6
29-Aug 0400	1.4642	6.0235	1.5	6
29-Aug 1400	1.5579	14.6286	1.0	5
20-Aug 1400	1.5773	5.6889	2.0	6
20-Aug 1600	1.9248	5.3895	1.6	5
20-Aug 1500	1.9349	12.8000	1.2	5
20-Aug 1700	1.9993	14.6286	2.1	5

Appendix D: Ocean current Conditions at the site

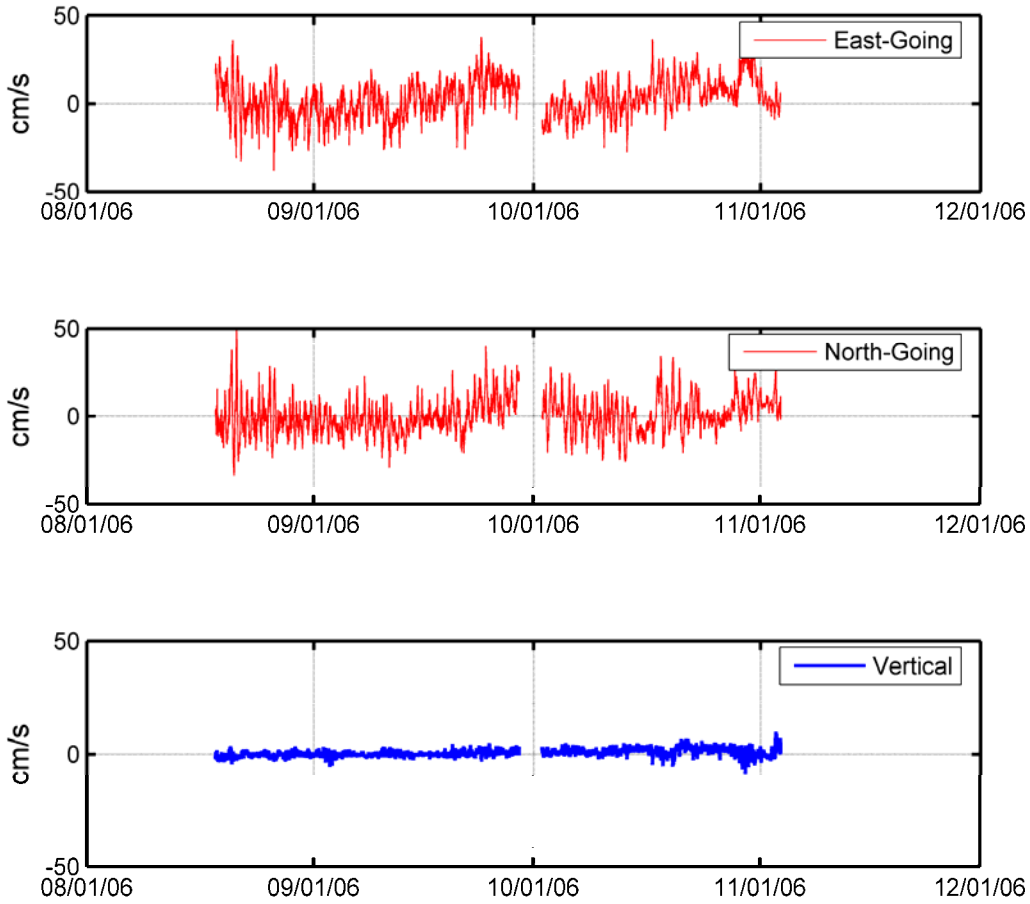

Figure D.1: The east- and north-going components of the measured velocities (also included in the vertical velocity component).

Table D.1: The highest 25 current velocity magnitude events recorded by the surface current meter (time is in UTC)

Date/Time	Speed (cm/s)	East-Going (cm/s)	North-Going (cm/s)
29-Oct 1245	37.0951	33.8915	15.0803
23-Sept 2030	37.1228	35.3805	11.2393
20-Aug 2215	37.2109	36.1303	-8.9024
21-Aug 1000	37.2580	-18.9368	32.0867
20-Aug 1945	37.2647	26.9745	25.7107
24-Sept 1200	37.3209	16.4970	33.4768
23-Sept 1945	37.4638	34.9808	13.4120
29-Oct 2145	37.8060	37.4078	5.4722
23-Sept 2000	38.1425	36.2090	11.9901
23-Sept 2100	38.1797	37.5932	6.6662
31-Oct 0100	38.4427	34.5202	16.9174
20-Aug 1845	38.5052	7.4009	37.7873
23-Sept 2015	38.9514	38.0024	8.5457
24-Sept 1130	38.9566	21.0535	32.7776
31-Oct 0115	39.3571	33.2663	21.0317
20-Aug 1900	39.8418	14.0875	37.2681
21-Aug 1115	40.4610	10.1286	39.1727
24-Sept 1145	40.6677	17.6964	36.6156
20-Aug 1915	41.2511	21.5206	35.1925
20-Aug 1930	41.3176	23.3960	34.0554
21-Aug 1100	41.3295	7.1017	40.7148
24-Sept 1115	42.7200	15.4483	39.8290
26-Aug 1245	43.2770	-37.9161	20.8632
21-Aug 1045	47.4085	4.8859	47.1561
21-Aug 1015	48.8230	-14.5816	46.5947
21-Aug 1030	50.3040	-3.6407	50.1721

Table D.2: The highest 25 events with a negative east-going velocity component (time is in UTC)

Date/Time	East-Going (cm/s)	North-Going (cm/s)
26-Aug 1245	-37.9161	20.8632
22-Aug 0045	-33.1387	6.0006
26-Aug 1300	-33.0222	16.7279
22-Aug 0100	-32.9892	12.8953
22-Aug 0115	-31.7391	17.7096
22-Aug 0200	-31.5931	16.8159
21-Aug 0915	-31.1768	17.5553
26-Aug 1230	-30.9823	13.1448
26-Aug 1315	-30.7359	13.0060
26-Aug 1215	-30.2415	-1.3924
21-Aug 0930	-29.4486	14.7157
22-Aug 0015	-28.8173	5.0280
21-Aug 0900	-28.5022	12.0729
13-Oct 1745	-27.8914	8.4018
26-Aug 1430	-27.8545	22.0142
22-Aug 0145	-27.7904	18.8133
22-Aug 0130	-27.3544	20.5965
29-Aug 0100	-27.1047	1.8725
31-Aug 0615	-27.0861	0.3202
21-Aug 0845	-26.7345	11.3210
29-Aug 0115	-26.7266	3.1204
29-Aug 0230	-26.7197	18.6973
13-Oct 1800	-26.5359	7.6385
10-Sept 1300	-26.4612	11.0859
22-Aug 0030	-26.3512	15.8930

Appendix E: Load Cell measurements during the deployment

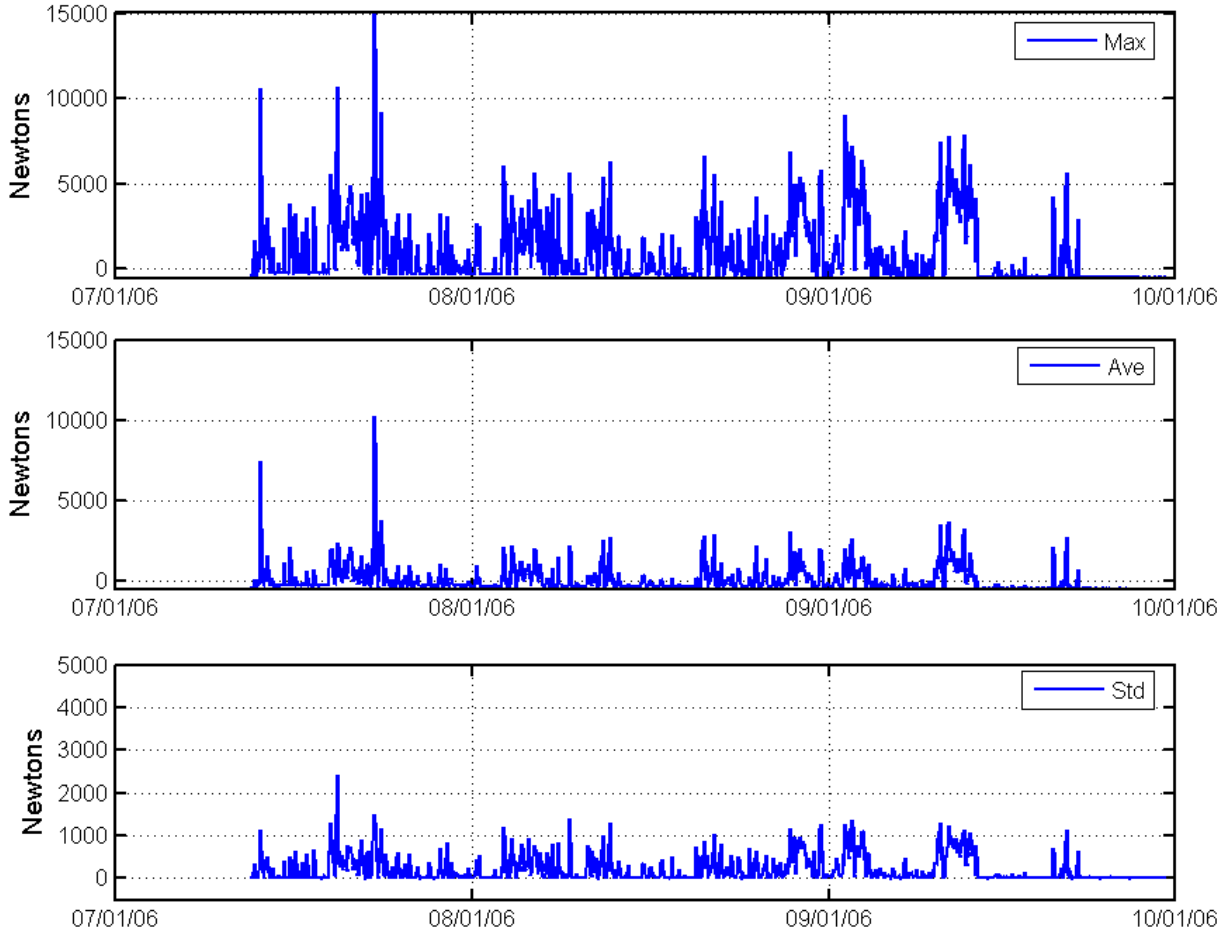

Figure E.1: The maximum, average and standard deviation from each of the 20 minute data sets obtained from the NE load cell.

Table E.1: The highest 25 tension events recorded by Load Cell NE

Tension (N)	Tension (lbf)	Day	Month	Year Time
6261	1408	12	Aug	2006 23:00
6354	1429	03	Sep	2006 01:00
6354	1429	03	Sep	2006 22:00
6372	1433	12	Sep	2006 16:00
6391	1437	03	Sep	2006 21:00
6502	1462	12	Sep	2006 18:00
6595	1483	21	Aug	2006 04:00
6595	1483	03	Sep	2006 02:00
6632	1491	02	Sep	2006 22:00
6669	1499	02	Sep	2006 21:00
6873	1545	28	Aug	2006 15:00
7059	1587	03	Sep	2006 00:00
7226	1626	02	Sep	2006 23:00
7430	1670	10	Sep	2006 16:00
7726	1737	23	Jul	2006 15:00
7782	1750	11	Sep	2006 10:00
7875	1770	12	Sep	2006 17:00
8209	1845	23	Jul	2006 11:00
9062	2037	02	Sep	2006 10:00
9210	2071	24	Jul	2006 03:00
10601	2383	13	Jul	2006 15:00
10694	2404	20	Jul	2006 07:00
10990	2471	23	Jul	2006 14:00
14514	3263	23	Jul	2006 12:00
15033	3380	23	Jul	2006 13:00

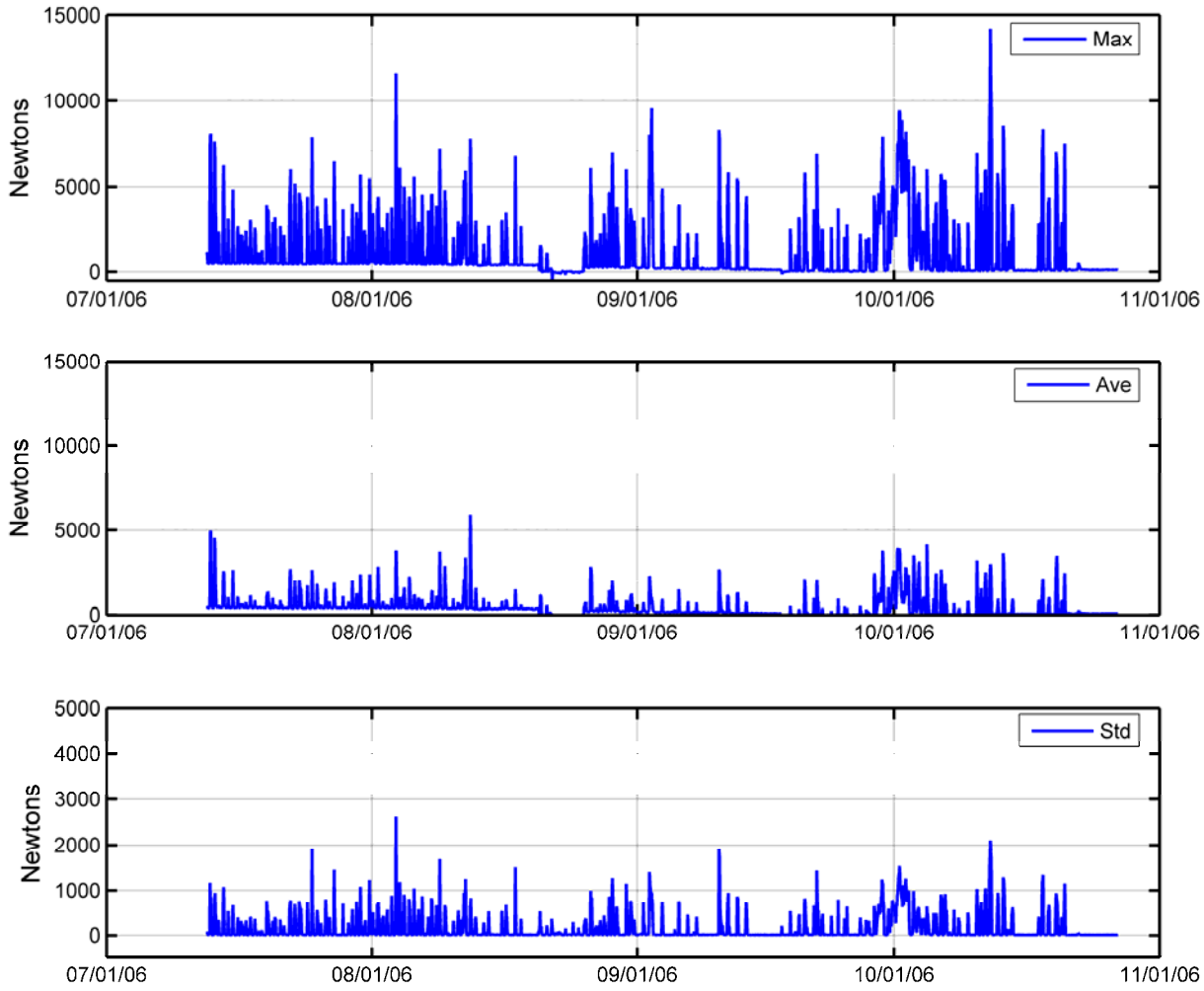

Figure E.2: The maximum, average and standard deviation from each of the 20 minute data sets obtained from the SE load cell.

Table E.2: The top 25 tensions recorded by Load Cell SE

Tension (N)	Tension (lbf)	Day	Month	Year	Time
7643	1718	01	Oct	2006	12:00
7643	1718	13	Oct	2006	19:00
7733	1739	02	Oct	2006	01:00
7787	1751	12	Aug	2006	12:00
7877	1771	25	Jul	2006	00:00
7877	1771	10	Sep	2006	14:00
7895	1775	13	Jul	2006	03:00
7913	1779	29	Sep	2006	16:00
8021	1803	02	Sep	2006	10:00
8093	1820	13	Jul	2006	04:00
8201	1842	02	Oct	2006	09:00
8309	1868	10	Sep	2006	13:00
8345	1876	18	Oct	2006	09:00
8561	1925	13	Oct	2006	18:00
8849	1990	01	Oct	2006	22:00
9209	2070	01	Oct	2006	16:00
9263	2083	01	Oct	2006	14:00
9425	2119	01	Oct	2006	15:00
9551	2147	02	Sep	2006	16:00
9731	2189	12	Oct	2006	05:00
9803	2204	12	Oct	2006	04:00
10523	2366	12	Oct	2006	08:00
10613	2386	12	Oct	2006	07:00
11621	2613	03	Aug	2006	19:00
14231	3199	12	Oct	2006	06:00

Appendix F: Wind speed and wave height time series from NDBC Stations I0SN3 and 44030

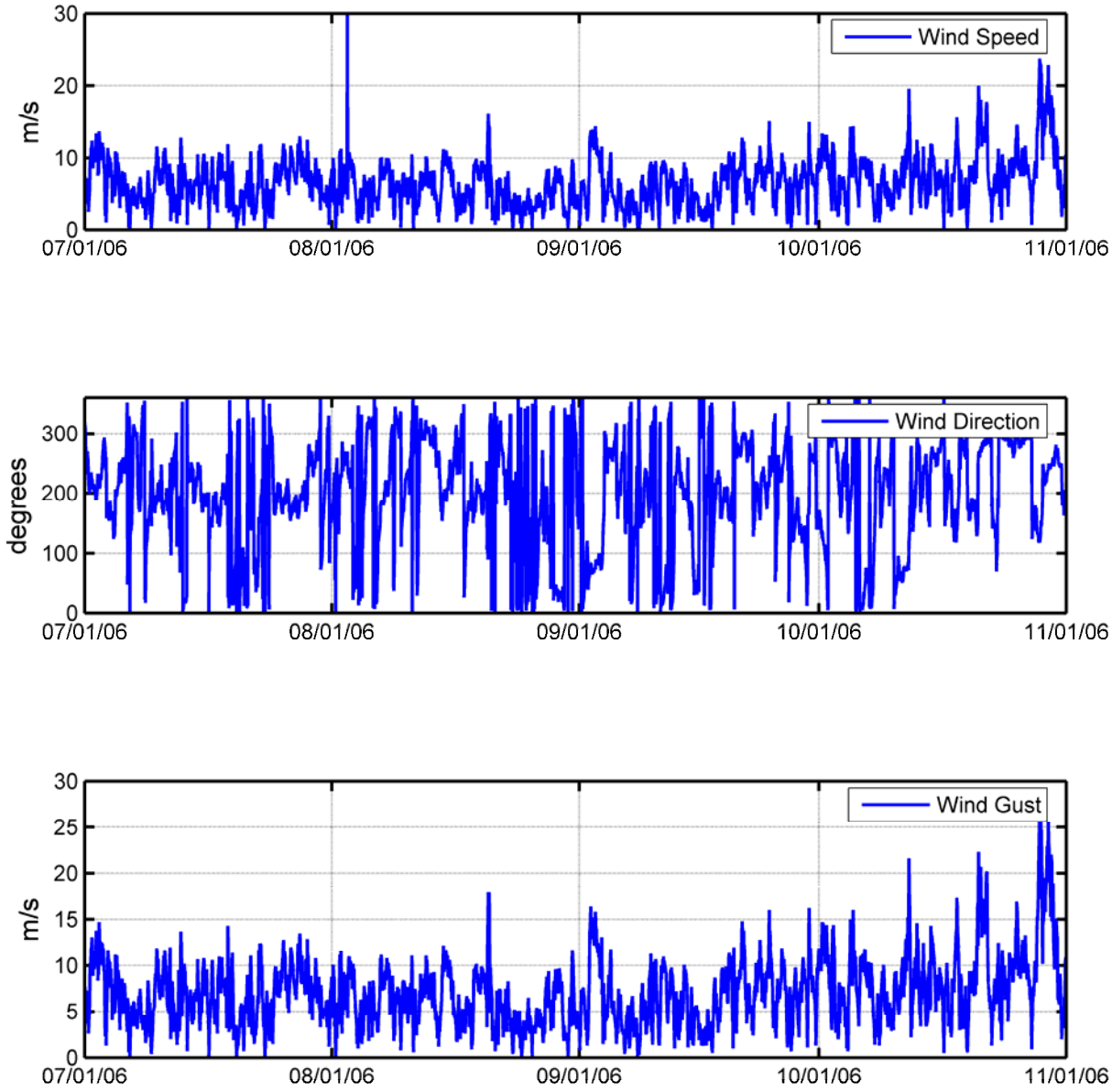

Figure F.1: The wind speed, direction and gust data sets from NDBC station I0SN3 from July through October.

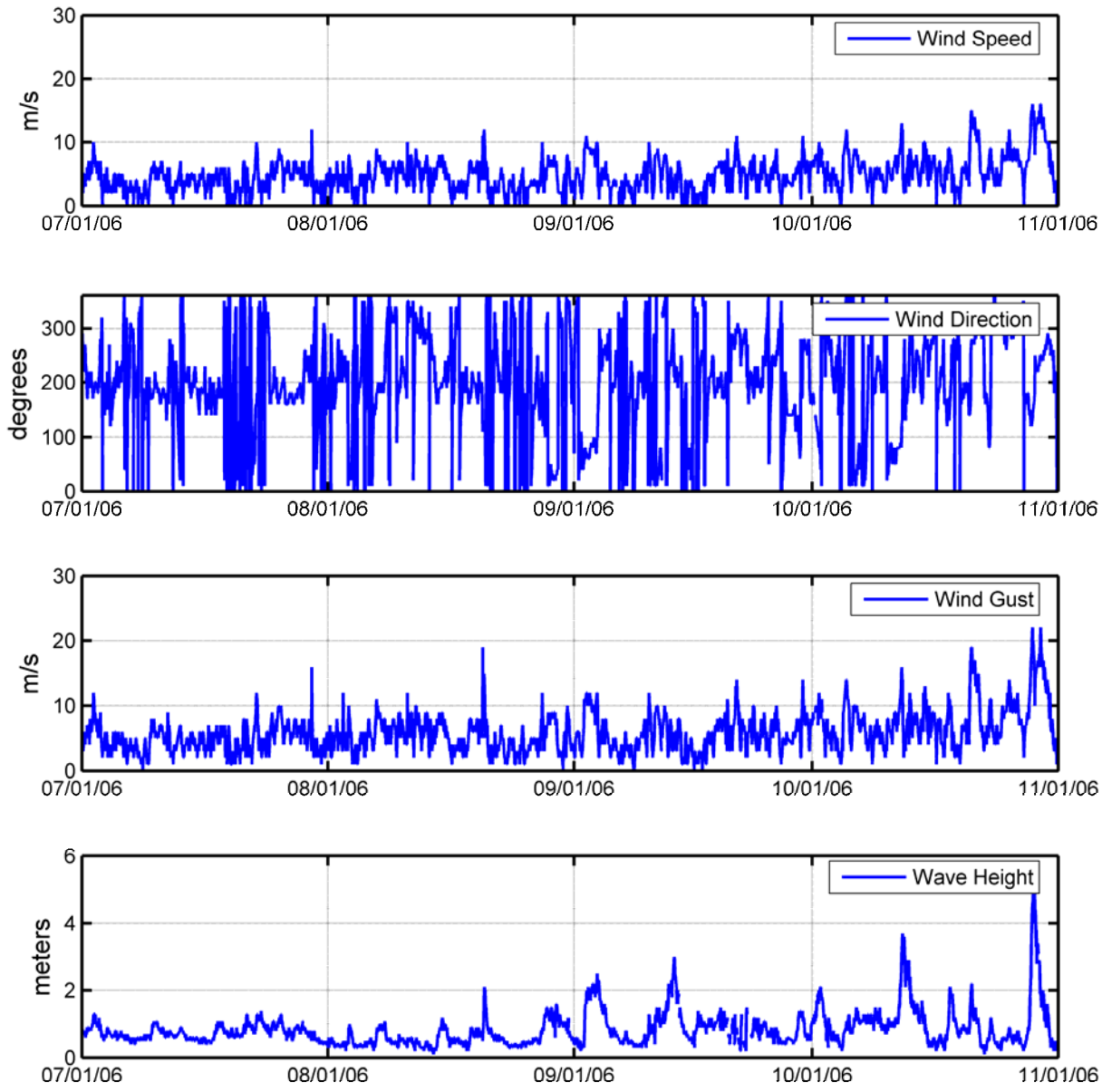

Figure F.2: The wind speed, direction gust and wave heights from NDBC Buoy 44030 from July through October